FINAL REPORT

For

Analysis of Auroral Particle Fluxes

August 1, 1973

Contract Number NASw-2212

Prepared by

C. R. Chappell

Lockheed Palo Alto Research Laboratory
3251 Hanover Street
Palo Alto, California 94304

For

National Aeronautics and Space Administration
Washington, D. C. 20546

CONTENTS

INTRODUCTION

Three Javelin rocket flights from Fort Churchill, Canada have provided detailed data on electron and proton precipitation in different types of auroral forms. These rockets named TWINS 1, TWINS 2, and ρ/α were launched in 1967 and 1968. A thorough understanding of auroral phenomena requires a high time resolution study of electron and proton energy spectra and pitch angle distributions with the ability to separate spatial and temporal effects. The TWINS 1 and 2 data furnish this necessary information and in addition study such things as the characteristics of the backscattered electrons and the transit times of the different energy auroral particles. Analysis of these data will give greater insight into the details of auroral production mechanisms. Under this contract these rocket data as well as pertinent satellite data measured in the magnetosphere will be studied to search for the mechanisms responsible for the auroral phenomena.

ACCOMPLISHMENTS

During the first year of the contract the TWINS data on precipitated and backscattered auroral electrons was compared with backscattered fluxes derived from a theoretical coulomb scattering analysis due to Walt, MacDonald, and Francis. It was found that the measured backscattered fluxes in the energy range of .5 keV to 2 keV often exceeded the theoretically predicted fluxes. This discrepancy can be explained by an electric field parallel to the magnetic field with a total potential drop of about 1 KV. Although this parallel field can substantially alter the characteristics of the precipitating auroral electrons, it is not of sufficient magnitude to act as the original source of these particles. A reprint from the Journal of Geophysical Research covering the details of this portion of the work is enclosed in this report.

During the second contract year we have pursued the details of the theoretically predicted backscattered electron fluxes. Our work has been directed toward combining the backscatter code of Walt et al. (1969) which is accurate down to energies of about 500 eV with a code devised by Banks and Nagy which was originally used to predict photoelectron fluxes both upgoing and downgoing in and above the neutral atmosphere. Dr. Nagy and Dr. Banks have worked to extend their code up to energies of 500 eV where it has been meshed with the higher energy results of Walt et al. This combined program is now able to predict the entire backscattered electron energy spectrum from auroral energies of 20 KeV down to a few eV. The combined computer code will also predict the height emission profiles of the important auroral optical emissions and can be used eventually to derive the auroral ionosphere created under a given arc.

A typical run of the combined program would be done as follows. Any given auroral spectrum covering the full energy range (a few eV to 10's of KeV) can be used as input. The portion of the spectrum greater than 500 eV is input into the Walt program. This program uses Coulomb scattering and the Bethe continuous energy loss formula to diffuse the particles in energy and pitch angle. It calculates the new distribution of degraded primaries as a function of energy (above 500 eV), pitch angle, and altitude. The degraded primary fluxes are then used directly with the neutral density profile and the appropriate ionization cross sections to calculate the secondary electrons produced at each altitude. These secondary electrons are then used as input for the low energy portion of the program. This part is computed using the Nagy-Banks portion with the initial energy spectrum below 500 eV and the secondaries as a function of altitude as the input. The Nagy-Banks portion of the program then calculates the transport and energy degradation of these secondary electrons, and the resulting distribution is used to calculate the different emission and ionization profiles.

The details of the combined auroral electron code are discussed in the attached preprint which has been submitted to the Journal of Geophysical Research. This paper shows many examples of incident auroral spectra and "monoenergetic" electron distributions. The spectral degradation, backscatter spectra, ionization rates, and optical emission profiles for these spectra are also shown. This preprint gives an excellent overview of the scope of the new auroral code which represents the bulk of the second year's contract effort.

During the fourth quarter of the second year the TWINS II data were examined for possible further comparison with the computational results of the newly developed program. In particular, a period toward the end of the flight in which the rocket penetrated the atmosphere in a nearly vertical direction was used to correlate the actually measured degrading electron spectrum with that calculated by the code. This approach proved to be unfeasible, however, because the temporal variations in the incident auroral spectrum were sufficiently great that they obscured the variations due to atmospheric degradation.

NEW TECHNOLOGY

The instruments discussed here were developed under previous NASA grants. Consequently there has been no new technology developed by this contract.

CONCLUSION

During the second year of this contract a significant new tool has been added to the study of auroral physics. The newly developed auroral electron code is now able to predict the scattering and energy loss of electrons covering the complete auroral energy spectrum from .5 eV up to several MeV. The code can be used very effectively in input-output experiments in which the incident auroral electron spectrum is measured by a satellite passing overhead and the resulting ionization or optical emissions are measured on the ground. The code will need to be continually refined to improve its accuracy and to expand its capabilities, but even in its present form it enables the modeling of the interaction of auroral electrons with the atmosphere to be done in a detailed way not previously possible, and consequently offers a major contribution to the study of the aurora and the ionosphere.

Twin Payload Observations of Incident and Backscattered Auroral Electrons

D. L. REASONER[1] AND C. R. CHAPPELL

Lockheed Palo Alto Research Laboratory, Palo Alto, California 94304

Energy spectra and pitch angle distributions of auroral electrons have been measured in a premidnight multiple arc auroral display by a Javelin rocket containing two identical payloads that separated in flight. The rocket (code-named Twins 2) was launched from Fort Churchill, Canada, at 0459 UT on March 2, 1968, and covered an altitude range up to 800 km. The electron energy spectra between 40 ev and 20 kev show a 'continuum' spectrum with a superimposed energetic peak. The center energy of the peak was observed to shift from 10–12 kev over the arcs to 2–3 kev between the arcs. This spectral structure is shown to be similar to the inverted 'V' structure reported by other investigators. The in flight separation of the two payloads allowed investigation of spatial versus temporal effects in the auroral precipitation. In one interval of the flight an arc was observed to be moving northward with a velocity of 0.6 km/sec. Calculated backscattered spectra are compared with those actually measured. Good agreement was observed for electron energies above about 1.5 kev, but below this energy the backscatter ratio was observed to be ~100%. Several explanations for this unusually high ratio are considered, and a likely possibility is shown to be a parallel downward-directed electric field between ~150 and 500 km.

Measurements of auroral particle fluxes, their spectra, and pitch angle distributions have been the object of numerous satellite and rocket investigations. A recent review of pertinent measurements has been given by *Paulikas* [1971].

The general features of auroral particle precipitation are now well known, although the details of the origins of the particles and of their interaction with the atmosphere are far from understood. Several investigators have reported 'anomalous' results in measurements of auroral particles. For example, *Mozer and Bruston* [1966*a*, *b*] reported energetic protons traveling upward from mirror points well within the atmosphere and anticorrelations between electron and proton fluxes. A recent study by *Rème and Bosqued* [1971] reported observations of anticorrelated proton and electron fluxes and proton pitch angle distributions peaked along field lines. These observations were interpreted as indicating the presence of electric fields parallel to magnetic field lines in the upper ionosphere with magnitudes ranging up to a few hundred millivolts/meter. Furthermore, *Mozer and Bruston* [1967] reported direct experimental evidence by means of rocket-borne electric field probes of such parallel electric fields in the upper ionosphere.

Choy and Arnoldy [1971] have observed an anomalously high reflection coefficient or backscatter ratio for auroral electrons with energies below 1 kev. These results are indeed surprising in view of the relatively low altitude of the measurements (<150 km, R. L. Arnoldy, private communication, 1972).

Chappell [1968] has compared calculated and measured auroral electron backscatter ratios using data from the Twins 1 twin payload sounding rocket [*Westerlund*, 1969]. The theoretical backscatter fluxes were calculated by means of a Fokker–Planck treatment of atmospheric Coulomb scattering. Discrepancies between calculated and measured backscatter were suggestive of atmospheric heating, a parallel electric field below the rocket, or a combination of both effects.

In this paper we report observations of precipitating ($30° < \alpha < 60°$) and backscattered ($120° < \alpha < 150°$) auroral electron fluxes in the energy range 40 ev to 20 kev over a series of IBC-2 auroral arcs. The measurements were

[1] Permanent address: Department of Space Science, Rice University, Houston, Texas 77001.

made with the Twins 2 payloads, a pair of identical payloads that were launched on an Argo D-4 Javelin sounding rocket and were separated in flight. Five distinct regions of particle precipitation are identified in terms of total energy input, and differing particle spectra characteristics are shown for each region. Variations in spectra near the edge of an arc are shown to resemble the 'inverted V' spectral structure [*Frank and Ackerson*, 1971]. Finally, measured and calculated backscatter spectra are compared, and an attempt is made to explain the observed discrepancies.

DESCRIPTION OF THE EXPERIMENT

A detailed description of the Twins 2 sounding rocket experiment and the auroral conditions at launch may be found in *O'Brien and Reasoner* [1971]. Briefly, the payloads were launched from Fort Churchill, Canada, on March 2, 1968, at 0459 UT into an IBC-2 northward-moving multiple arc structure. The ground magnetometers recorded a 100-γ negative bay at the time of the flight.

The rocket carried two identical payloads, Twins 2A and 2B, which were separated in flight with a relative velocity along the flight direction at separation of approximately 4 m/sec. The relative and absolute velocities perpendicular to the magnetic field lines were 1 ± 0.2 m/sec and 585 ± 6 m/sec, respectively. The flight azimuth was 37° east of true north. Auroral electron spectra were measured over an altitude range of 200–800 km, and the payloads covered L values from $L \cong 9$ to $L \cong 13$.

Each payload carried identical detector complements, consisting of two wide range electron spectrometers, three fixed-energy differential electron detectors, and a large-area Geiger tube. Of relevance to this study were the two electron spectrometers, code-named Specs[*O'Brien et al.*, 1967]. The Specs detectors were electrostatic deflection spectrometers employing channel electron multipliers and were sensitive to electrons with 40 ev $< E <$ 20 kev. The Specs were laboratory calibrated both by an electron beam and by placing a calibrated ^{63}Ni source over the apertures, thereby establishing the relative efficiencies of the upward- and downward-looking instruments. The upward-looking Specs scanned a pitch angle range of 30°–60° in ~5° increments, and the downward-looking Specs simultaneously scanned a range of 120°–150°. The Specs required 3.6 sec to complete a measurement cycle of all electron energies. Payload aspect information was provided by a flux gate magnetometer.

EXPERIMENTAL RESULTS

An overview of the auroral conditions encountered during the Twins 2 flight is best shown by a plot of the total energy deposited, obtained by integrating over the measured spectra. Figures 1 and 2 show the values of the directional electron energy deposited and backscattered as calculated from the measurements of Twins 2A and 2B, respectively, for electron energies >400 ev and pitch angles of $30° < \alpha < 60°$ and $120° < \alpha < 150°$. The payloads encountered two distinct periods of enhanced precipitation at 240–350 sec and again at 670–710 sec. We can associate these periods of enhanced precipitation with the visible auroral arcs. The precipitated fluxes were isotropic to within a factor of 2–3 over the pitch angle range $30° < \alpha < 60°$. When it is assumed that the isotropy extended over the upper hemisphere, the total energy deposited was therefore ~20 ergs/cm^2 sec. This agrees well with the photometrically measured brightness of the auroral forms at launch of 10–20 kR.

The gross features of Figures 1 and 2 are in good agreement, as would be expected, since the maximum payload separation was 700 meters. The backscattered flux measured by Twins 2A

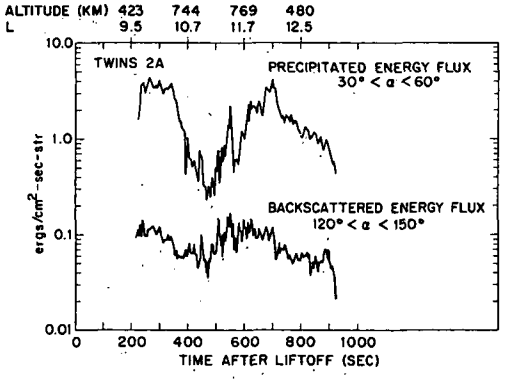

Fig. 1. Total directional incident and backscattered electron energy flux measured by Twins 2A. The measurements were computed by integrating the measured electron spectra, appropriately weighted, over the energy range 400 ev to 20 kev.

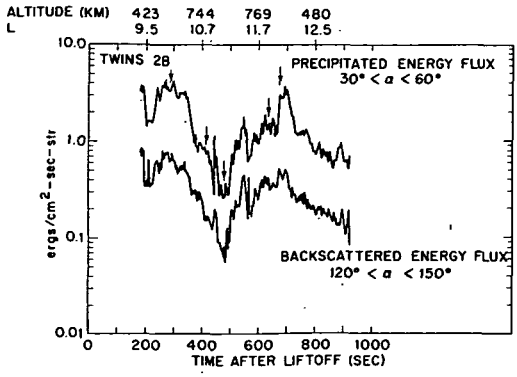

Fig. 2. Total directional incident and backscattered electron energy flux measured by Twins 2B. The measurements were computed by integrating the measured electron spectra, appropriately weighted, over the energy range 400 ev to 20 kev.

is apparently less than that measured by Twins 2B, but this was due to a failure of two of the six channels of the downward-looking Specs on Twins 2A. Therefore, part of the electron spectrum was not measured by this detector. The general characteristics of both incident and backscattered particle spectrums as measured by both payloads were similar throughout the flight, thus increasing our confidence in the data presented herein. We have elected to concentrate on spectrums measured by Twins 2B because of the partial failure of the Twins 2A downward-looking Specs.

A closer examination of Figures 1 and 2 reveals that the decrease in precipitation at $T = 350$ sec was observed 6 ± 3 sec earlier by Twins 2B (the following payload) than by Twins 2A (the leading payload). This means that the arc observed from 250 to 350 sec was moving northward more rapidly than the payloads and effectively overtook and ran ahead of them. Considering the payload absolute horizontal velocity of 0.585 km/sec and the separation at this time of 217 meters, the arc is calculated to be moving northward with a velocity along the payload flight direction (37° east of north) of 0.61 km/sec. Flux enhancements later in the flight (e.g., $T = 630$ sec) do not display any time delays between detection by the two payloads, although the Specs detectors with their 3.6-sec cycle time would not have been able to resolve the time delay of ~2 sec expected if the payloads encountered a stationary or slowly moving spatial structure. It is therefore possible that the payloads initially observed a northward-moving arc, which subsequently slowed and was again encountered by the northward-moving payloads. The unique capability of the Twins payloads to distinguish temporal and spatial effects demonstrated above was also instrumental in the discovery of short-duration field-aligned electron bursts reported previously by *O'Brien and Reasoner* [1971].

Figures 3–8 show precipitated and backscattered electron spectra measured at various times in the flight by Twins 2B. These spectra represent regions of differing precipitation intensity at $T = 281$, 414, 479, 630, and 670 sec. These times are indicated by the arrows in Figure 2. Each spectrum represents an average over 3 Specs cycles, or about 10 sec. The periods were selected to insure that there were no fluctuations in the data, which exceeded the usual variations due to statistics. Each point is an average of 147 samples of 10 msec each with the 147 points divided (by the Specs switching sequence) into three groups of forty-nine 10-msec samples.

Figure 3 shows the incident, or precipitated, spectrum at $T = 281$ sec. The fluxes in units of el/cm² sec ster ev are plotted as a function of electron energy in electron volts. This spectrum was measured at an altitude of 585 km and represents pitch angles of 32°–56°. The loss cone (referenced to the 100-km level) at 585

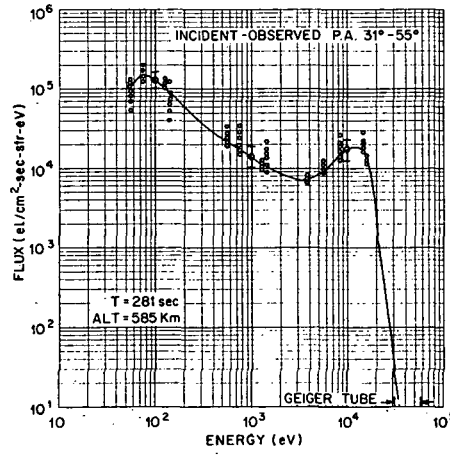

Fig. 3. Incident electron energy spectrum measured at $T = 281$ sec. For reference with regard to the time of measurement for this figure and Figures 4–9, see Figure 2.

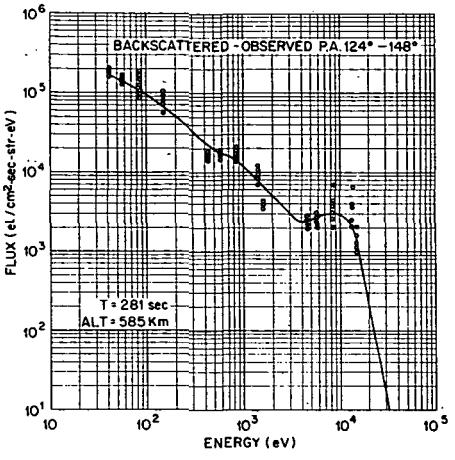

Fig. 4. Backscattered electron energy spectrum measured at $T = 281$ sec.

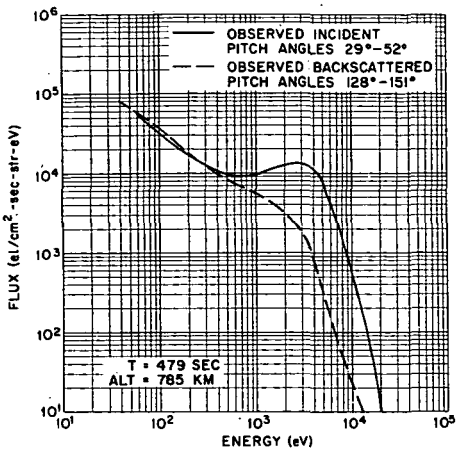

Fig. 6. Incident and backscattered electron energy spectra measured at $T = 479$ sec.

km is 64°, and hence all of the observed incident electrons would theoretically mirror below 100 km and thus be subject to severe atmospheric scattering and loss. All downgoing electrons measured throughout the flight were in the loss cone; hence no information on the trapped-particle population was acquired. The group of data points at each energy represents the spread in flux at a given energy for different pitch angles betwen 32° and 56° and indicates the variation of energy spectrum with pitch angle. This variation is a factor of 2 to 3 maximum. The error bars for the points are also indicated. The errors are dominated by uncertainties in the instrument calibration of ±20%. Errors due to counting statistics are negligible, typically <5%. The precipitating electrons shown in Figure 3 have a peak in the energy range of 6–17 kev, which contains the bulk of the total precipitating energy.

Figure 4 shows the electron spectrum that was backscattered from the atmosphere below the payload as measured simultaneously at $T = 281$ sec by the downward-viewing Specs. The data format is the same as that for Figure 3. The pitch angle range measured was 124°–148°. Note that the backscattered spectrum exhibits a small peak in the range 5–15 kev, which is

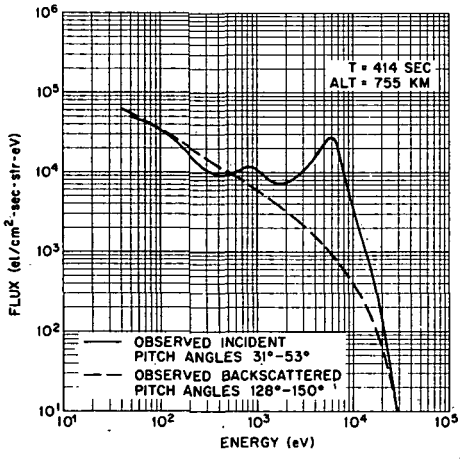

Fig. 5. Incident and backscattered electron energy spectra measured at $T = 414$ sec.

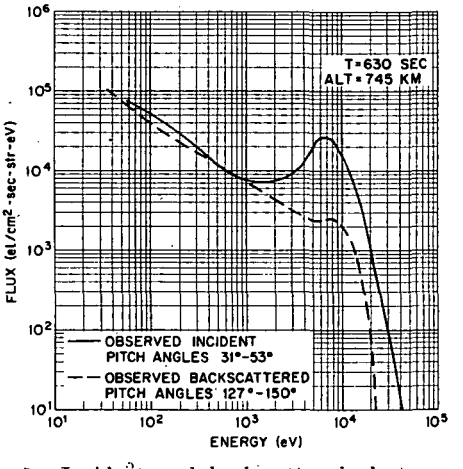

Fig. 7. Incident and backscattered electron energy spectra measured at $T = 630$ sec.

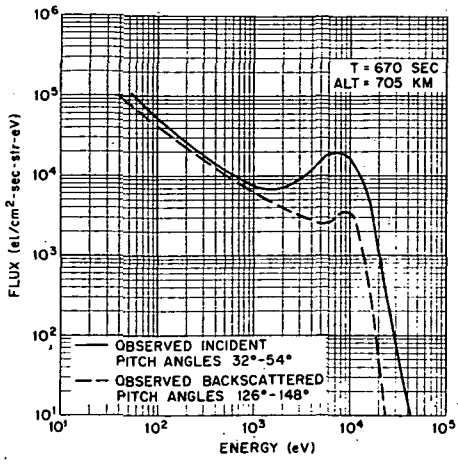

Fig. 8. Incident and backscattered electron energy spectra measured at $T = 670$ sec.

almost an order of magnitude lower in intensity than the precipitated flux.

As the payloads passed from the region of intense precipitation into one of intermediate precipitation ($T = 414$ sec), the spectra changed to those shown in Figure 5. Here we have shown only the sketched incident and backscattered spectra without including the data points showing the spread in pitch angle. This is done here and in subsequent presentations for the sake of brevity and to afford easier comparison of spectra.

The incident spectrum at $T = 414$ (solid line) shows two peaks, a prominent peak in the range 2–9 kev and a less prominent one in the range 500 ev to 1.2 kev. This last peak, although it was not observed consistently throughout the flight, is nonetheless a real feature representing enhancements relative to the 'continuum' in two adjacent energy channels with a difference of greater than 3 standard deviations. Note that, as the payloads passed out of the region of enhanced precipitation (Figure 3), the peak shifted down from 6–17 kev to 2–9 kev. The backscattered spectrum (dashed line) shows no evidence of a peak. Note also that the flux of backscattered electrons with $E < 600$ ev is comparable to or greater than the corresponding flux of precipitating electrons. We will comment further on this surprising backscatter ratio in a later section.

Figure 6 shows the incident and backscattered spectra in the region of low-intensity precipitation at $T = 479$ sec. The peak in the incident spectrum has shifted to the energy range 1.5–4 kev and has diminished in differential flux level by a factor of 2 from the previous spectrum. This precipitated spectrum measured between the intense precipitation regions is similar to the background continuum discussed by *Westerlund* [1969] using data from Twins 1, a similar rocket payload fired 1 year earlier. Here, the backscattered spectrum shows no peak in energy, unlike the backscattered spectrum in the intense precipitation region ($T = 281$ sec, Figure 4). Again, the backscatter ratio is ~100% for energies less than 500 ev.

Following the low-intensity region the rocket encountered another region of intermediate intensity precipitation with the incident electron energy spectrum showing a characteristic upward shift in the energy of the peak to the 3- to 12-kev range. Figure 7 shows representative spectra from this region measured at $T = 630$ sec. The backscattered spectrum has a slight peak in this same energy range. In this case the backscatter ratio is ~100% for energies less than 1.2 kev.

Finally, the payloads again encountered a region of intense precipitation (Figure 8) at $T = 670$ sec. The energy of the peak is in the 3- to 16-kev range, and the incident spectrum is similar to that observed during the first enhanced period at $T = 281$ sec. This adds support to the thesis advanced earlier that the two regions of intense precipitation were one and the same arc. The backscatter peak is again prominent, and the backscatter ratio is ~100% for energies below 1 kev.

From this series of spectra it is clear that changes in the total energy deposited were caused by shifts in the energy of an energetic peak that appeared to be superimposed on a much more stable continuum spectrum. During this Twins 2 flight, unlike the case in the Twins 1 flight [*Westerlund*, 1969], the peak never completely disappeared, although it was considerably diminished in both intensity and average energy in the period of $T = 460$ to $T = 500$ sec.

A higher time resolution study of this peak shift effect is shown in Figure 9. Here three successive incident spectra at $T = 351$, $T = 366$, and $T = 405$ sec are plotted to display the spectral change over the time period of a

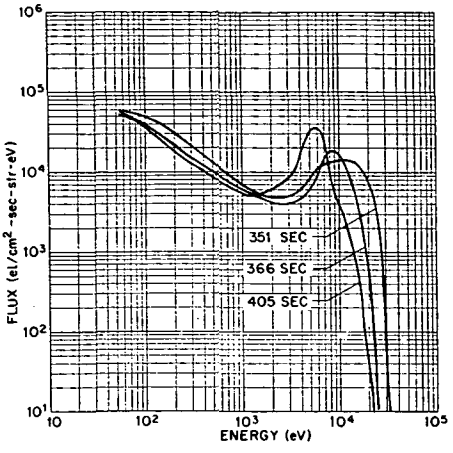

Fig. 9. A series of three incident electron energy spectra measured in the period $T = 351$ to $T = 405$ sec showing the shift in the energy of the peak as the payload exits the region over an auroral arc.

sharp decrease in total precipitating intensity (Figure 1). The shift of the energy of the peak to progressively lower values is clearly evident. We will discuss this further in a later section.

Perhaps the most surprising feature of these spectra is the very high, ~100%, backscatter ratio for electron energies less than about 1 kev. The expected ratio computed from Coulomb scattering is usually of the order of 10%. In the following section we consider the backscatter phenomena in detail, presenting calculations of expected backscattered fluxes for comparison with those actually observed.

Comparison of Experimental and Theoretical Backscatter Results

To examine the interaction of the precipitated auroral electrons with the atmosphere, we have used the measured incident electron spectrum as input for a theoretical computer code that calculates the expected backscattered electron spectrum. This calculated backscattered spectrum can then be directly compared with the backscattered spectrum measured simultaneously by the downward-viewing Specs detector on the Twins payload. Any differences between the calculated and measured backscattered spectra can be interpreted in terms of the physical processes occurring in the interaction region.

The theoretical calculations were made using the Fokker-Planck diffusion equation solution of *Walt et al.* [1968]. This treatment includes angular scattering, continuous energy loss, and the effect of a converging magnetic field. The solution is in the form of a distribution function for the auroral electrons as a function of energy, pitch angle, and altitude. The calculations were made using differential cross sections given by the first Born approximation [*Mott and Massey*, 1965] and the continuous energy loss formula of *Bethe* [1933]. These calculations are reasonably accurate ($\pm 10\%$) for isotropic pitch angle distributions and for electron energies down to about 500 ev. The computations done in this work are carried down to 1 kev.

Figure 10 shows the measured incident (solid line) and backscattered (circles) spectra at $T = 281$ in the first region of enhanced precipitation. The incident spectrum, which was assumed to be isotropic in pitch angle over the upper hemisphere, was used as input to the backscatter code. The dotted area represents the calculated backscattered flux in the range of pitch angles of 126°–149° corresponding to the pitch angles measured by the downward-viewing Specs. The agreement between the calculated backscattered flux and the measured flux (circles) is reasonably good above about 1.5 kev. However, below 1.5 kev the measured backscattered fluxes are roughly equal in magnitude to the incident fluxes (backscatter ratio of

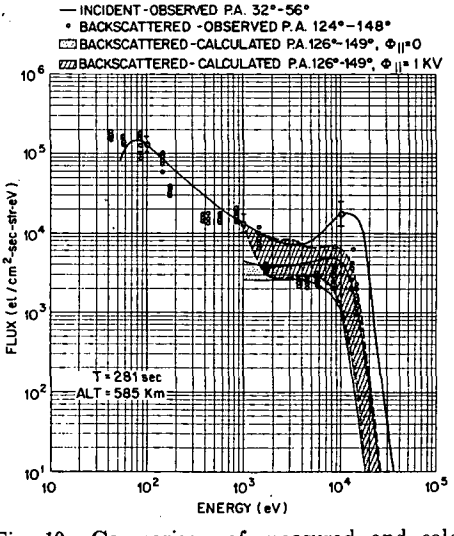

Fig. 10. Comparison of measured and calculated backscattered electron spectra at $T = 281$ sec, a region of intense precipitation.

~100%). The theoretical calculations, which employ Coulomb scattering only, predict a backscatter ratio more on the order of 10–20%, not 100%. In other words, the electrons of energy below 1–2 kev in this enhanced precipitation region are either kept out of the atmosphere preventing any loss or the incident primary particles are replaced by secondaries produced in atmospheric scattering.

One obvious explanation for the 100% backscatter below 1–2 kev is the presence of a parallel downward-directed electric field above the atmosphere with a total potential drop of about 1 kv in magnitude. This field would prevent electrons of less than 1 kev from entering the atmosphere and would reflect them undiminished in flux value. Other potential explanations also exist for this unusually high backscatter ratio. The production of multiple secondary electrons in the atmosphere by the energetic precipitating primaries is a possibility. Also, a severe modulation of the magnetic field by the auroral electrojet currents could possibly affect the particle pitch angles and cause reflection. In anticipation of the results of a later discussion on the relative merits of these possibilities, we will examine theoretically the effect of a parallel downward-directed electric field of potential drop of 1 kv situated below the rocket and above the effective scattering layer of the neutral atmosphere. In this $T = 281$ case this field would be between 585 km and about 150 km.

For this $T = 281$ case we have again used the measured incident spectrum shown in Figure 10 but have included a vertical potential drop $\Phi_{\parallel}$ of 1 kv just below the rocket. The effect of this parallel field is to alter the pitch angle distribution of the incident particles in such a way as to reflect particles whose energy component parallel to the field is less than 1 kev and to reduce the energy of particles that traverse the field region by 1 kev. The Coulomb scattering, energy loss, and mirroring of these penetrating electrons are then calculated by the computer code, and the resulting backscattered spectrum is then transformed back through the potential drop with the corresponding change in pitch angle distribution and increase in energy. The results of this calculation are shown by the shaded area in Figure 10 for energies down to 1 kev. Note that the effect of the field is to increase the flux backscattered at the more nearly perpendicular pitch angles for electrons between 1 and ~10 kev in energy and also to cause the 100% backscatter below energies of a few kev. Qualitatively then, the calculations show that, with the addition of a parallel downward-directed electric field above the atmosphere to the general effects of Coulomb scattering, the predicted backscattered flux is in good agreement with the measured backscattered flux for all energies.

Figure 11 shows the measured and calculated backscattered fluxes for the time period of very low intensity precipitation, $T = 479$ sec. As before, the measured incident spectrum is shown by the solid line and is used as the input for the calculation. The shaded area shows the predicted range of backscattered flux for the pitch angles measured by the downward-viewing Specs. The measured backscattered electrons are again shown by the circles. In this calculation we have not included a parallel electric field. One can see that the agreement above 1 kev for Coulomb scattering is quite good. Recall that this set of spectra was measured between the auroral arc regions. Although no parallel electric field is required to obtain agreement between calculated and observed backscattered spectra above 1 kev in this low-intensity precipitation region, one can see that below about 500 ev the backscattered flux again approximately equals the incident flux, indicating the

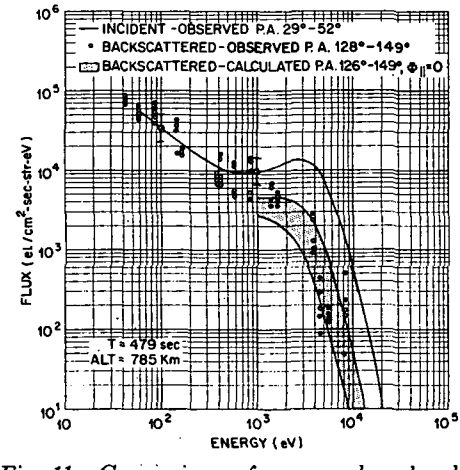

Fig. 11. Comparison of measured and calculated backscattered electron spectra at $T = 479$ sec, the time of the minimum precipitation.

possible need for a lower-magnitude parallel field with potential drop of about 500 volts to give agreement.

Figure 12 shows the set of spectra representing the second payload encounter with the intense precipitation region at $T = 670$ sec. Again, the shaded area represents the predicted backscattered fluxes with no parallel electric field, and the circles represent the measured backscattered fluxes. As in the first case ($T = 281$), the agreement at higher energies (greater than about 1.5 kev) is good. However, as in the previous encounter with the intense precipitation region, the backscattered fluxes below about 1.5 kev are comparable to the incident fluxes in contrast with the predictions of the Coulomb scattering calculations, which show the backscattered flux decreasing with decreasing energy below 1.5 kev. As before, one can see that the addition of a parallel electric field of about 1-kv total potential drop below the rocket would cause an increase in the predicted backscattered fluxes at lower energies (less than about 6 or 8 kev) with a backscattered flux equal to the incident flux below about 1.5 kev, in agreement with the measured fluxes.

We have found then that in regions of auroral precipitation the measured backscattered electron fluxes agree quite well with the backscattered fluxes predicted from Coulomb scattering alone for the higher energies greater than about 1.5 kev. However, for the lower energies, agreement between predicted and measured backscattered fluxes for Coulomb scattering alone is not sufficient but requires an effect such as a parallel downward-directed electric field between the rocket and the atmosphere with a total potential drop of about 1 kv in regions of intense precipitation and about 500 volts in regions of less intense precipitation.

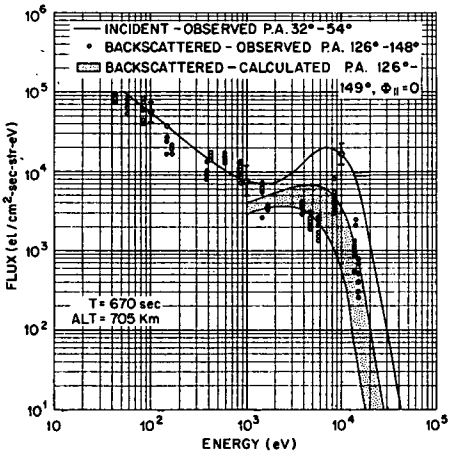

Fig. 12. Comparison of measured and calculated backscattered electron spectra at $T = 670$ sec, a period of intense precipitation.

Summary and Discussion

The features of the measured precipitated and backscattered auroral electron spectra can be summarized as follows.

1. The spectra contain two main components, a continuum spectrum that remains fairly stable throughout the flight and a peak in the 6- to 17-kev range, which is present over the auroral arcs but which shifts to lower energy and intensity as the payloads move away from the arc. This peak, when it is present, carries the bulk of the total energy deposited.

2. The incident electron fluxes at all energies appear to be isotropic in pitch angle to within a factor of 2 or 3 over the observed pitch angle range of 30°–60°.

3. The backscattered fluxes for energies below about 1 kev appear to be isotropic within a factor of 2 or 3 and equal in intensity to the precipitated fluxes. Above about 1 kev the fluxes show a larger variation with pitch angle as expected from the effects of atmospheric scattering and the magnitude of the backscatter ratio ($j(E)$ up/$J(E)$ down) at a given energy decreases with increasing energy.

4. A theoretical backscatter calculation employing Coulomb scattering, continuous energy loss, and magnetic mirroring and using the measured incident spectrum as input is able to reproduce the measured backscattered spectrum for energies greater than 1.5 kev in intense regions of precipitation and for energies of greater than 500 ev in regions of less intense precipitation. The measured backscattered spectra below about 1.5 kev, however, cannot be explained on the basis of Coulomb scattering alone.

In the first feature above we mentioned the shift in energy of the peak in the incident electron spectrum as the payloads move in and out of the auroral arc region. If this shift in peak energy were displayed on an energy-time spec-

trogram, it would resemble an inverted V structure similar to that discussed by *Frank and Ackerson* [1971]. The widths of the structures observed here (50–100 km) are in reasonable agreement with the 'typical' widths of 200 km discussed by *Frank and Ackerson* [1971]. Exact agreement on these widths is not expected owing to uncertainties resulting from high velocities of the auroral forms relative to the rocket payload velocities.

The most interesting feature of the electron spectra is the 100% backscatter ratio for energies less than 1.5 kev. As we mentioned in the previous section, there are at least three possible explanations for this large ratio: secondary electrons that are produced by the high-energy primary electrons and that are scattered upward out of the atmosphere, a large variation in the ambient magnetic field caused by the nearby auroral electrojet that changes the electron pitch angles, or a downward-directed parallel electric field with a potential drop of 1 kv above the atmosphere, which reflects lower-energy electrons before they undergo scattering.

We discount the possibility that secondary electrons are responsible for the upward fluxes at energies between 40 ev and 1 kev. If these particles were secondaries, we would expect that the measured upward flux of these particles would be correlated with the measured incident primary energy flux of the particles greater than 400 ev. In Figure 13 we show the incident energy flux from Figure 1 along with the 40-ev precipitated and backscattered number flux. There is a good correlation between the 40-ev downgoing and upcoming flux, but there is no significant correlation between the precipitated primary energy flux and the 40-ev upcoming or backscattered flux. Thus the experimental evidence argues against secondary electrons as a source of these low-energy electrons.

Theoretical evidence also argues against secondaries as a source of the high-intensity low-energy influx. Most of the secondaries that are produced are below 300 km, and the calculations of *Nagy and Banks* [1970] show that these electrons cannot escape the atmosphere because of the very high degree of scattering. However, these same calculations show that a 50-ev electron produced at an altitude greater than 300 km can escape significant scattering and travel freely upward. Cross sections for secondary

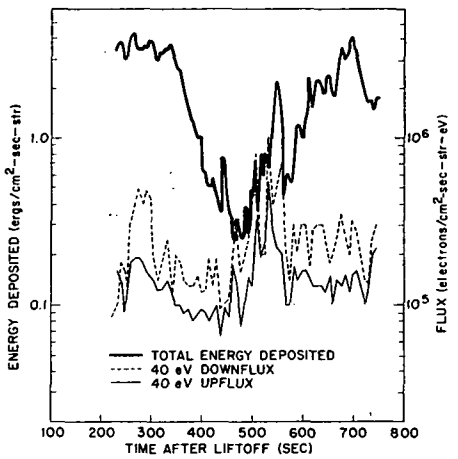

Fig. 13. A comparison of the total incident energy flux (from Figure 1) with the measured 40-ev incident and backscattered flux.

electron production by energetic primary electrons incident on N_2 have been measured by *Opal et al.* [1971]. Taking the integrated N_2 density above 300 km for a medium density atmosphere as 2×10^{15} atoms/cm² [*Johnson*, 1965] and the precipitated energy as 3 ergs/cm² sec ster with an average energy of 10 kev, we compute the expected upward secondary flux at 40 ev from above 300 km of 0.2×10^5 el/cm² sec ster ev. This is just about equal to the change seen in the 40-ev upward flux in the time period of $T = 340$–440 sec as the primary energy flux drops from about 3 ergs/cm² sec ster to 0.4 erg/cm² sec ster. Therefore, although secondary electron production above 300 km appears to contribute to the upflux of low-energy electrons, its contribution is only a minor part of the total observed upflux (0.2×10^5 el/cm² sec ster ev out of about 1.5×10^5 el/cm² sec ster ev).

Recent calculations by A. F. Nagy (private communication, 1972) have shown that the backscatter ratio below 40 ev can exceed 100% owing to backscattered and secondary electrons. However, above 40 ev the ratio falls off smoothly to the 20% value of 500 ev shown by the present calculations.

As in the case of the secondary electrons, we can also rule out the possibility of magnetic field perturbations as a cause of the large backscatter ratios. First, invariant calculations show that an increase of a factor of more than 3 in

the ambient magnetic field is required to cause a particle with a pitch angle of 30° at 585 km to mirror above the neutral atmosphere. Magnetic field changes of this magnitude are not observed in the vicinity of aurorae.

After discounting secondary electrons and magnetic field perturbations, the obvious explanation remaining is the presence of a parallel downward-directed electric field below the rocket of potential drop about 1 kv. A field of this sort would cause the incident auroral electrons with energies less than 1–2 kev to mirror above the region of significant scattering in the atmosphere. The backscatter calculations of the previous section have shown that the addition of such a field would give good agreement between calculated and observed backscattered electrons.

There are, however, certain crucial limitations on this electric field that must be met in this case. The first is that a total potential drop of ~1 kv must exist between the rocket altitude and the top of the scattering region (about 150 km for 1-kev electrons). The second is that there appears to be no large fraction of this potential drop above 500 km, for there was not a systematic large variation with altitude of the lowest-energy flux in the altitude range 500–800 km. Thus for the purpose of discussion we postulate a parallel electric field with a total potential drop of about 1 kev located between 150- and 500-km altitude.

Recent experimental and theoretical investigations have provided a possible source for the postulated electric field. *Zmuda et al.* [1966], *Cloutier et al.* [1970], and *Choy et al.* [1971] have inferred the presence of field-aligned currents composed of very low energy electrons flowing out of the auroral ionosphere. *Kindel and Kennel* [1971] have theoretically investigated the effects of these currents and have concluded that ion acoustic and ion cyclotron instabilities, which are driven by the field-aligned currents, can occur under the conditions found in the auroral ionosphere. The role of the instabilities is to furnish an impedance to the flow of field-aligned currents and hence to cause a potential drop to develop.

There is, however, a certain difficulty with the application of this mechanism to our particular case. For the range of field-aligned current values expected just from flux balance in the aurora studied here (10^8–10^9 el/cm² sec), an examination of Figure 7 of *Kindel and Kennel* [1971] shows that the first instability expected would be the O^+ or H^+ ion cyclotron mode and then only at altitudes greater than 1000 km. We require that the electric field, and hence the instability region, exist below 500 km. A possible explanation for this apparent inconsistency is as follows. The critical current for instability is not only a function of altitude but also of the electron to ion temperature ratio. As the electrons are heated in relation to the ions, ion Landau and cyclotron damping become less important in stabilizing the waves. An examination of Figure 2 of *Kindel and Kennel* [1971] shows that, if the ratio of electron drift velocity to electron thermal velocity is initially above a certain value ($V_d/V_{th} \sim 0.03$ for $T_e/T_i = 1$), increasing the T_e/T_i ratio will cause waves to grow. Therefore, if the electrons in the 150- to 500-km region could be heated sufficiently, the instabilities and hence the electric fields would exist and be confined to this region. Possible mechanisms for accomplishing this heating include an energy transfer from secondary electrons by means of electrostatic waves (the 'bump on tail' instability) or an upward transport of hot electrons from below.

The above argument is necessarily qualitative, for data on crucial parameters such as temperature and drift velocity of the electrons contributing to the field-aligned currents are lacking. It is offered here as a plausible explanation for the required altitude structure of the postulated parallel electric field. Whatever the precise cause, the existence of the parallel downward-directed electric field appears necessary to adequately explain the data shown above.

CONCLUSIONS

The physical processes that describe the interaction of auroral electrons with the atmosphere appear to be more complex than just the Coulomb scattering of the incident primary electrons with a subsequent loss of energy. The comparison of the measured backscattered electron spectra with spectra predicted using a theoretical scattering calculation has led to a discrepancy for energies below about 1–2 kev. It was found that the very high ratio (~100%) of backscattered to incident fluxes for these energies could most reasonably be explained by

a parallel downward-directed electric field that prevents these lower-energy electrons from entering the atmospheric scattering region. This parallel field with potential drop of about 1 kv is thought to have its origin in wave-particle interactions in the turbulent auroral ionosphere.

Acknowledgments. We are grateful to Dr. B. J. O'Brien for his initiation and development of the Twins payload concept and to Dr. L. Westerlund, Mr. J. Sneddon, Mr. F. Abney, and Mr. R. Harrison for their work on the Twins payload. We are also grateful to Dr. Martin Walt for helpful discussions during the course of the data analysis and to Mr. A. J. Fernandez for his help with the computer codes.

This work was funded under contract NASw 2212 from the National Aeronautics and Space Administration.

* * *

The Editor thanks L. A. Frank and G. A. Paulikas for their assistance in evaluating this paper.

REFERENCES

Bethe, H., Elektronentheorie der Metalle, in *Handbuch der Physik,* vol. 24, part 1, edited by A. Snekal, chap. 3, Springer Verlag, Berlin, 1933.

Chappell, C. R., The interaction of auroral electrons with the atmosphere, Ph.D. thesis, Rice Univ., Houston, Tex., 1968.

Choy, L. W., and R. L. Arnoldy, Charged-particle measurements over an auroral arc (abstract), *Eos Trans. AGU, 52,* 895, 1971.

Choy, L. W., R. L. Arnoldy, W. Potter, P. Kintner, and L. J. Cahill, Jr., Field-aligned particle currents near an auroral Arc, *J. Geophys. Res., 76,* 8279–8298, 1971.

Cloutier, P. A., H. R. Anderson, R. J. Park, R. R. Vondrak, R. J. Speiger, and B. R. Sandel, Detection of geomagnetically aligned currents associated with an auroral arc, *J. Geophys. Res., 75,* 2595–2600, 1970.

Frank, L. A., and K. L. Ackerson, Observations of charged-particle precipitation into the auroral zone, *J. Geophys. Res., 76,* 3612–3643, 1971.

Johnson, F. S., Structure of the upper atmosphere, in *Satellite Environment Handbook,* edited by F. Johnson, p. 17, Stanford University Press, Palo Alto, Calif., 1965.

Kindel, J. M., and C. F. Kennel, Topside current instabilities, *J. Geophys. Res., 76,* 3055–3078, 1971.

Mott, N. F., and H. S. W. Massey, *The Theory of Atomic Collisions,* 3rd ed., Clarendon, Oxford, 1965.

Mozer, F. S., and P. Bruston, Observation of the low-altitude acceleration of auroral protons, *J. Geophys. Res., 71,* 2201–2206, 1966*a*.

Mozer, F. S., and P. Bruston, Properties of the auroral-zone electron source deduced from electron spectrums and angular distributions, *J. Geophys. Res., 71,* 4451–4467, 1966*b*.

Mozer, F. S., and P. Bruston, Electric field measurements in the auroral ionosphere, *J. Geophys. Res., 72,* 1109–1114, 1967.

Nagy, A. F., and P. M. Banks, Photoelectron fluxes in the ionosphere, *J. Geophys. Res., 75,* 6260–6270, 1970.

O'Brien, B. J., F. Abney, J. Burch, R. LaQuey, R. Harrison, and T. Winiecki, Specs, a versatile space-qualified detector of charged particles, *Rev. Sci. Instrum., 38,* 1058, 1967.

O'Brien, B. J., and D. L. Reasoner, Measurements of highly collimated short-duration bursts of auroral electrons and comparison with existing auroral models, *J. Geophys. Res., 76,* 8258–8278, 1971.

Opal, C. B., E. C. Beaty, and W. K. Peterson, Tables of energy and angular distributions of electrons ejected from simple gases by electron impact, *Rep. 108,* Joint Inst. for Lab. Astrophys., Univ. of Colo., Boulder, Colo., 1971.

Paulikas, G. A., The patterns and sources of high-latitude particle precipitation, *Rev. Geophys. Space Phys., 9,* 659–702, 1971.

Rème, H., and J. M. Bosqued, Evidence near the auroral ionosphere of a parallel electric field deduced from energy and angular distributions of low-energy particles, *J. Geophys. Res., 76,* 7683–7693, 1971.

Walt, M., W. M. McDonald, and W. E. Francis, Penetration of auroral electrons into the atmosphere, in *Physics of the Magnetosphere,* edited by R. Carovillano and J. F. McClay, p. 534, Reinhold, New York, 1968.

Westerlund, L. H., The auroral energy spectrum extended to 45 ev, *J. Geophys. Res., 74,* 351–354, 1969.

Zmuda, A. J., J. H. Martin, and F. T. Heuring, Transverse magnetic disturbances at 1100 kilometers in the auroral region, *J. Geophys. Res., 71,* 5033–5054, 1966.

(Received August 23, 1972;
accepted January 4, 1973.)

A New Model for the Interaction of Auroral Electrons With The Atmosphere; Spectral Degradation, Backscatter, Optical Emission and Ionization

P. M. Banks[1]
C. R. Chappell
Lockheed Palo Alto Research Laboratory
Palo Alto, California 94306

A. F. Nagy
Dept. of Electrical and Computer Engineering
University of Michigan
Ann Arbor, Michigan

July 1973

[1] Permanent Address:

Dept. of Applied Physics and Information Sciences
University of California, San Diego
La Jolla, California 92037

ABSTRACT

A new computational model has been created to describe the interaction of auroral electrons with the atmosphere. For electrons of energy greater than 500 eV continuous energy losses and small angle deflections are combined in a Fokker-Planck diffusion equation which computes energy spectrums over all pitch angles throughout the atmosphere. These fluxes are then used to determine the rates of secondary electron and degraded ($E < 500$ eV) primary electron production at all heights. This information is used to compute upward and downward hemispherical fluxes in the energy range 0 to 500 eV taking into account discrete energy losses, large angle scattering and particle transport along magnetic field lines. The model has been used to compute energy spectrums, ionization rates, backscatter ratios and optical emissions associated with different incident electron spectrums. For monoenergetic electrons of energy 2 keV and above the results obtained agree well with the work of Rees (1969) and Rees and Maeda (1973). At lower energies the effects of transport and elastic collisions become progressively more important and the present results differ significantly both from the Rees and Maeda results and those obtained from the ideas of energy degradation. Finally, spectrums typical of the nighttime auroral oval and daytime polar cusp are used to obtain the altitude dependent fluxes, ionization rates and optical emissions.

I. Introduction

There have been many previous attempts to provide an accurate description of the way auroral electrons interact with the earth's upper atmosphere (see Rees, 1969 for a comprehensive review). The models resulting from these studies have become increasingly sophisticated in the past decade as new information about the various ionization and excitation processes has become available. In addition, there has been a parallel improvement in our knowledge of the different aspects of the aurora itself, not only in terms of the nature of the incident electron energy and angular spectrums but also the different effects within the atmosphere; i.e., the time and space variations of electron density and ion composition, the altitude variation of various optical emissions, the structure of the electron flux at different heights, and so forth.

To a large extent many of the different models of auroral electron behavior developed in the past have been based upon the ideas of energy deposition and, as a consequence, cannot be relied upon to accurately describe secondary ionization, dissociation, and other similar collisional interactions which depend upon the electron flux at energies less than 500 to 1000 eV. In an effort to improve this situation a new computational model has been developed to describe the penetration of auroral electrons into the upper atmosphere. This model incorporates both continuous and discrete energy losses while taking into account the

motions of electrons of all energies along the magnetic field, the various effects of elastic and inelastic collisions, and the presence of secondary electrons arising from collisional ionization.

The first widely used model of auroral electron penetration, developed by Rees (1963), was based upon laboratory data for the range and energy deposition rate of electrons in air obtained by Grün (1957). Using an empirical expression based on the laboratory results, Rees computed the primary fluxes and the atmospheric ionization rate as a function of altitude for incident electron energies greater than 400 eV and for arbitrary pitch angles. In a later study, Stolarski (1968) also used the Grün data to calculate the primary electron fluxes, secondary ionization rates and optical emissions. Monte Carlo techniques were first used by Maeda (1965) and Stadsnes and Maehlum (1965) for calculating the behavior of auroral electrons by considering continuous electron energy losses and angular scattering of many test electrons over a range of incident pitch angles. Certain results of the later Monte Carlo computations of Berger et al. (1970) were used by Rees (1969) to create a new computational model but, for various reasons, the results of this hybrid method have been criticized (Shemansky, et al., 1972) and further work has been necessary to overcome these difficulties (Rees and Maeda, 1973).

A different approach to the problem of auroral electrons was taken by Walt et al., (1969) who used a Fokker-Planck diffusion equation to describe simultaneously electron energy degradation, electron angular

scattering through collisions with the atmospheric gases and the effect of the earth's converging magnetic field upon the electron pitch angle distribution. In the method of Walt, et al., the incident auroral electron flux is described in terms of the pitch angle and energy distributions. As the electrons pass into the atmosphere, analytic expressions for the energy loss (based on the Bethe formula) and angular scattering (based on the Born approximation) are used to compute the energy distribution and compute angular distributions (over both the upper and lower hemispheres) of the particles as a function of altitude.

Although there are certain advantages associated with the work of Rees, Walt, et al., Rees and Maeda, Berger and Seltzer and others, their methods share the problem that of any description of electron energy loss or angular scattering based upon continuous energy loss and small angle scattering becomes increasingly poor below 500 eV. Thus, while the behavior of electrons having energies greater than 500 eV can be accurately done using the expressions developed for a small fractional energy loss per collision, as one goes to energies below 500 eV the discrete nature of collisions in terms of energy loss and angular scattering becomes of crucial importance. Although attempts have been made to compute separately the low (0 to 100 eV) energy portion of the secondary electron spectrum (Rees, et al., 1969), such an approach ignores the contribution of the energy degraded primary flux and leaves unresolved questions about the details of the electron flux between 100 and 500 eV. In

addition such methods neglect the possibility of low energy electron transport along the magnetic field lines.

Several years ago a new model of low energy electron behavior was introduced (Banks and Nagy, 1970; Nagy and Banks, 1970, 1971) in a study of the processes affecting the energy and space distributions of electrons created through atmospheric photoionization caused by absorption of solar EUV radiation. In this model two-stream continuity equations were used to describe electron fluxes moving into and out of the atmosphere along magnetic field lines. Discrete energy losses and angular scattering were explicitly included in terms of appropriate energy dependent cross-sections. Although this computational model was originally intended to describe photoelectrons, it can be used equally well to describe the lower energy portion of the auroral electron energy spectrum.

In the following sections a new model of auroral electron behavior based upon continuous energy losses at high energies ($E > 500$ eV) and discrete losses at low energies ($E < 500$ eV) is described. For high energies the Fokker-Planck diffusion approach of Walt et al., (1969) has been adjusted with a revised Born approximation (Chappell, 1968) to cover energy loss and angular scattering for electron energies as low as 500 eV. Below 500 eV a discrete energy loss description based upon the method of Banks and Nagy (1970) and Nagy and Banks (1970) is used which takes into account the incident low energy particles, the energy degraded primary particles and the secondary electrons created through impact ionization.

The computer code resulting from the joining of the two methods gives complete energy spectrums of auroral electrons throughout the atmosphere in terms of the upgoing and downgoing electron fluxes. From these electron fluxes it is possible to compute ionization rates for the different neutral gases, the rates of various optical excitations, and other pertinent quantities.

II. The Computational Model

Discrete excitation and ionization processes involving outer shell electrons dominate electron energy losses at low energies where the cross sections, while not known in complete detail, can be fairly well represented through simple analytic expressions described later. Above about 500 eV, however, progressively greater uncertainty is present with regard to specific processes involving both inner and outer shell electrons of the atmospheric gases. Further, as the electron energy increases, the fractional incident electron energy loss per collision decreases and the discreteness of the various losses becomes less important in describing the passage of electrons through the atmosphere. For the present model the joining point between the discrete and the continuous descriptions of electron energy loss has been taken as 500 eV. While somewhat arbitrary, this choice reflects a compromise between computer data storage capacity and the accuracy of the continuous loss description at electron energies lower than 1 keV. (A more complete discussion of this point is given later.) In the following paragraphs descriptions are given of the continuous and discrete models.

Continuous Losses: Electron Energies Greater than 500 eV:

To describe the behavior of electrons having energies greater than 500 eV the Fokker-Planck diffusion equation approach of Walt et al., (1969) has been used. In this model a magnetic field geometry with $B \propto R^{-3}$ is assumed to account for the effects of magnetic mirroring. The elastic scattering cross sections with the atmospheric gases are obtained by calculating the deflection of the incident electron by the Coulomb field of a charged scattering center. The atomic structure is relatively unimportant in this approximation and the differential scattering cross section can be written as

$$\sigma(\beta,\theta) = \frac{Z^2e^4}{4m^2c^4} \frac{(1-\beta^2)}{\beta^4} \frac{[1-\beta^2\sin^2\theta/2]}{\sin^4\theta/2} \qquad (1)$$

where θ is the scattering angle, Z is the scattering center charge, m and e are the electron mass and charge, $\beta = v/c$, and c is the speed of light. The principal source of elastic scattering at high energies (E > 10 keV) arises from interaction with the nucleus; scattering collisions with the orbital electrons are relatively unimportant. At lower energies (1) must be modified to include the effects of orbital electrons. Such modification has been described by Chappell (1968) giving

$$\sigma(\beta,\theta) = \frac{e^4}{4m^2c^4}(Z-F(\theta))^2 \frac{(1-\beta^2)}{\beta^4} \frac{[1-\beta^2\sin^2\theta/2]}{\sin^4\theta/2} \qquad (2)$$

where $F(\theta)$ is an atomic scattering factor which introduces the shielding

effect of the orbital electrons on the scattering of lower energy ($E < 10$ keV) primaries. Values for $F(\theta)$ are tabulated in the International Tables for X-ray Crystallography (1962).

For the energy loss of the incident electrons, scattering by orbital electrons dominates and the Bethe formula is used in the form

$$\frac{dT}{dx} = - \frac{4\pi e^4}{m^2 c^4 \beta^2} \sum_j n_j \ell n \left(T\, mc^2 \sqrt{2.7(T+2)} \,/2I_j \right) \qquad (3)$$

where T is the electron kinetic energy in rest mass units, I_j is the average excitation energy of the j-th species target atom (see Table 1) and n_j is the number density of bound electrons in the j-th atmospheric gas.

Using equations (2) and (3), Walt, et al., (1969) developed a Fokker-Planck diffusion equation to describe the passage of an incident electron flux through the atmosphere. The computations involve numerical solutions for the steady state electron distribution function with calculations being made of the electron flux as a function of altitude, energy and pitch angle. The input parameters for the model include the incident electron energy spectrum ($E > 500$ eV) and the initial pitch angle distribution.

As auroral electrons move into the atmosphere they are continually degraded in energy and eventually must either be backscattered out of the atmosphere or pass through the computational threshold of 500 eV into the lower energy regime where the Bethe formula approximation of continuous

energy loss cannot be maintained. The energy degraded electrons are produced at all altitudes in both upgoing and downgoing directions with a characteristic energy spectrum extending from 250 eV up to 500 eV with the precise energy dependence of the production rate at a given altitude reflecting the energy loss processes acting at energies above 500 eV. Although the altitude variation of the degraded primary electron production rate is proportional to the energy dissipation rate of the primary flux, it is necessary to note that these electrons are free to travel along the magnetic field to deposit their energy and create optical excitations in regions separated from their point of origin.

The incident high energy electron flux is also responsible for collisional ionization and the creation of secondary electrons. Like the degraded primary electrons, the secondary electrons are free to travel along field lines undergoing various inelastic and elastic collision processes. To model the production rate of the secondary electrons created through ionization impact collisions an analytical expression obtained from the work of Opal, et al., (1971) has been used. If $S(E_p,E_s)$ is the partial cross section describing the creation of a secondary electron in the range energy E_s, $E_s + dE_s$ by an electron originally possessing kinetic energy E_p, the results of Opal, et al., can be approximated by the expression

$$S(E_p,E_s) = \frac{2}{\pi\tilde{E}} \frac{\sigma_i(E_p)}{1 + (E_s/\tilde{E})^2} \qquad (4)$$

where $\sigma_i(E_p)$ is the ionization cross section at energy E_p and $\tilde{E}$ is an empirically obtained energy degradation coefficient. Values of $\tilde{E}$ for N_2, O_2 and O are given in Table 2.

To model the ionization cross section as a function of electron energy the series of analytical expressions developed by A.E.S. Green and his collaborators have been used (Stolarski, personal communication, 1972. See also Green & Stolarski, 1972). From this work the total electron impact ionization cross section can be written as

$$\sigma_i(E_p) = q_o A \int_I^{(E_p+I)/2} \frac{\epsilon^{-\Omega}}{W^2} \left[1 - e^{-\gamma}\right]^{\nu} dW \qquad (5)$$

where $q_o = 6.51 \times 10^{-14}$ cm^2 eV^2, I is the ionization potential of a particular state of the final ion, A is an empirical parameter, W is the energy loss of the primary particle, $\epsilon = E_p/W$ and Ω, γ and ν are chosen to permit (5) to fit experimental ionization cross-sections.

The integration limits of (5) are chosen to accommodate the definitions of degraded primary and secondary electrons. In an ionization collision two electrons share what remains of the original incident electron kinetic energy (E_p-I) between them. The electron having kinetic energy in the range $(E_p-I)/2$ to (E_p-I) is referred to as the degraded primary electron while the electron having kinetic energy in the range 0 to $(E_p-I)/2$ is the secondary electron. If the primary electron loses an energy W, it follows that the secondary electron has an energy W-I. A sketch of the way secondary and primary electrons are distributed in

energy as a result of a flux of electrons of energy E_p is shown in Figure 1.

Closed expressions corresponding to (5) can be obtained when ν is an integer (see Table 3 for parameter values for N_2, O_2 and O):

O: $\nu = 1$ $\sigma_i(E_p) = G(A-B)$

N_2: $\nu = 2$ $\sigma_i(E_p) = G(A-2B+C)$

O_2: $\nu = 3$ $\sigma_i(E_p) = G(A-3B+3C-D)$

where

$$A = \frac{\left(\frac{\epsilon+1}{2}\right)^{\Omega-p-1} - 1}{\Omega - p - 1}$$

$$B = \left[\frac{\left(\frac{\epsilon+1}{2}\right)^{\Omega+\gamma-p-1} - 1}{\Omega + \gamma - p - 1}\right] \epsilon^{-\gamma}$$

$$C = \left[\frac{\left(\frac{\epsilon+1}{2}\right)^{\Omega+2\gamma-p-1} - 1}{\Omega + 2\gamma - p - 1}\right] \epsilon^{-2\gamma}$$

$$D = \left[\frac{\left(\frac{\epsilon+1}{2}\right)^{\Omega+3\gamma-p-1} - 1}{\Omega + 3\gamma - p - 1}\right] \epsilon^{-3\gamma}$$

and $\epsilon = E_p/I$, $G = \frac{q_o A}{I} \epsilon^{-\Omega}$.

Using the data of Table 3, ionization cross sections for the atmospheric gases can be computed from threshold to large, but non-relativistic, energies.

From the foregoing comments it follows that in addition to the incident low energy ($E < 500$ eV) flux at high altitudes, there are two sources for the low energy flux within the atmosphere which arise from the passage of high energy ($E > 500$ eV) electrons through the neutral gases; i.e., the production of secondaries and degraded primaries. The altitude and energy dependent production rates for secondaries and degraded primaries can be obtained from (4) once the spectrum of the $E > 500$ eV electrons is known and a model atmosphere has been adopted. To illustrate this, the $E < 500$ eV production rate obtained for a typical nighttime auroral spectrum (discussed in a later section) is shown in Figure 2 as a function of electron energy for several altitudes. Owing to the form of the incident electron spectrum the simple symmetry shown in Figure 1 is absent since the production of secondaries dominates the production of degraded secondaries.

Discrete Losses: Electron Energies Less Than 500 eV:

For energies less than 500 eV the fractional energy loss per collision becomes large and the effects of large angle elastic scattering arising from incident electron-orbital electron interactions cannot be ignored. Electron flux calculations for the low energy portion of the spectrum are made using the two stream continuity equations described by Banks

and Nagy (1970), Nagy and Banks (1970) and Stolarski (1972). In this method the transport of electrons along the magnetic field lines is described in terms of the hemispherical fluxes of two electron streams Φ^+ (upwards) and Φ^- (downwards). These fluxes are defined as

$$\Phi^+(E,z) = \int_{\substack{\text{Upper}\\\text{Hemisphere}}} \phi(E,z,\Omega)d\Omega \tag{6}$$

$$\Phi^-(E,z) = \int_{\substack{\text{Lower}\\\text{Hemisphere}}} \phi(E,z,\Omega)d\Omega \tag{7}$$

where $\phi(E,z,\Omega)$ is the electron flux per unit energy and solid angle at the altitude z.

The continuity equations for Φ^+ and Φ^- can be derived by considering: (a) inelastic collisions (energy degradation) with forward and backscattering and (b) elastic scattering (no significant energy degradation) with forward and backscattering and (c) the production of electrons in a given energy range. When it is assumed that gravity, electric fields parallel to magnetic field lines, and the effects of magnetic field convergence can be neglected, the steady state continuity equations for Φ^+ and Φ^- can be written as

$$\frac{d\Phi^+}{ds} = \frac{-1}{\langle\cos\theta\rangle}\sum_k n_k\left[\sigma_a{}^k + p_e{}^k\sigma_e{}^k\right]\Phi^+ + \frac{1}{\langle\cos\theta\rangle}\sum_k n_k p_e{}^k\sigma_e{}^k\,\Phi^- + q/2\langle\cos\theta\rangle + q^+/\langle\cos\theta\rangle \tag{8}$$

$$-\frac{d\Phi^-}{ds} = \frac{-1}{\langle \cos\theta \rangle} \sum_k n_k \left[\sigma_a{}^k + p_e{}^k \sigma_e{}^k \right] \Phi^- + \frac{1}{\langle \cos\theta \rangle} \sum_k n_k p_e{}^k \sigma_e{}^k \Phi^+$$

$$+ q/2\langle \cos\theta \rangle + q^-/\langle \cos\theta \rangle \qquad (9)$$

where

$$\sigma_a{}^k = \sum_i \sigma_{ai}^k$$

$$q^+(E,s) = \sum_k n_k(s) \sum_{\epsilon > E} \left| p_{aj}^k(E') \sigma_{aj}^k(E' \to E) \Phi^-(E',s) \right.$$

$$\left. + (1 - p_{ai}^k(E') \sigma_{aj}^k(E' \to E)\ \Phi^+(E',s) \right|$$

$$q^-(E,s) = \sum_k n_k(s) \sum_{\epsilon > E} \left| p_{aj}^k(E') \sigma_{aj}^k(E' \to E)\ \Phi^+(E',s) \right.$$

$$\left. + (1 - p_{aj}^k(E') \sigma_{aj}^k(E' \to E) \Phi^-(E',s) \right|$$

and

s, distance along a magnetic field line (positive outward).

$\Phi^+(E,s)$, electron flux upward along s

$\Phi^-(E,s)$, electron flux downward along s

$n_k(s)$, kth neutral species number density

$p_e{}^k(E)$, electron backscatter probability for elastic collisions with the kth neutral species

$\sigma_e{}^k(E)$, electron total scattering cross section for elastic collisions with the kth neutral species

$q(E,s)$, electron production rate in the range E to E + dE due to ionization processes; ie, the production of secondary electrons, the energy degraded primaries falling in the range 250 to 500 eV and, if necessary, the presence of photoelectrons created through the absorption of ultraviolet radiation.

$q^{\pm}$, electron production in the range E to E + dE due to cascading from higher energy electrons undergoing inelastic collisions.

$p_{a_j}^k$, electron backscatter probability for collisions with the kth neutral species resulting in the jth inelastic process.

$\sigma_{a_j}^k$, inelastic cross section for the jth excitation of the kth neutral species.

To take into account pitch angle effects an average pitch angle $\langle \cos \theta \rangle$ has been introduced into (8) and (9); a pitch angle of 68° has been used in the calculations presented later.

The cross sections and parameters used in the present calculations have been taken from Green and Stolarski (1972)and Stolarski (personal communication, 1972). The formulas describing ionization processes have been already given by equation (4) and (5), and Tables 3 and 4 list the ionization cross section parameters used.

The analytic form of the cross sections describing electron impact excitation of atomic and molecular states is taken from Green and Stolarski (1972) as

$$\sigma_a(E) = \frac{q_o A_o}{W^2} \left[1 - \frac{W}{E}\right]^{\nu} \left(\frac{W}{E}\right)^{\Omega} \qquad (10)$$

where $q_o = 6.51 \times 10^{-14}$ cm^2 eV^2, W is the excitation energy and E is the incident electron energy. Table 5 lists the adopted values of the excitation parameters.

The cross sections for elastic collisions for energies less than 100 eV have been discussed previously by Nagy and Banks (1970). Table 6 lists the values adopted here for the range $100 < E < 500$ eV. The elastic cross sections for O were taken from Sunshine, et al. (1967) while the values of Fisk (1936) were used for O_2 and N_2. For electron-thermal electron collisions the revised energy transfer rates of Schunk and Hays (1971) have been adopted.

The elastic and inelastic backscatter probabilities are important parameters but, unfortunately, information about them is very sparse (see McDaniel, 1964; Mott and Massey, 1965; Kieffer, 1967; Lassettre, 1969; Shyn, et al., 1972, and Opal et al., 1971). The elastic backscatter probabilities measured for N_2 by Shyn, et al., (1972) were adopted for both N_2 and O_2 elastic and excitation collisions. The backscattering probabilities for O calculated by Fink and Yates (1970) have been used for both the elastic and excitation processes. For ionization processes it is assumed that the primaries continue in the same direction while the secondary electrons are distributed isotropically.

To a large extent the success of the present method depends upon the matching of energy loss rates in passing from the continuous to the discrete regimes. A comparison of these energy loss rates is shown

for N_2 in Figure 3. The dotted curve is derived from the discrete processes given in Tables 3 and 5 while the solid curve follows from the Bethe formula of equation (3). At progressively lower energies the Bethe formula is first too large, then much smaller than the discrete losses. At the 500 eV boundary used here the Bethe energy loss formula value is 2.9% larger than the sum of the discrete losses. For O_2 and O the discrepancies are 7.4% and 1.8%, respectively.

Method of Solution

The computed auroral electron flux is obtained from sequential solutions to the Fokker-Planck diffusion equation and the low energy, two stream continuity equations. After the incident auroral energy spectrum and pitch angle distribution has been adopted, the electron flux for $E > 500$ is computed as a function of pitch angle, energy and altitude. These fluxes are then used to determine, at each altitude, the rate of production of $E < 500$ eV degraded primary and secondary electrons.

In the second step, the two stream continuity equations are solved using an implicit integration technique. The lower boundary condition for these equations, taken deep in the atmosphere, is $\Phi^+(E,z\to 0) = \Phi^-(E,z\to 0) = 0$ for all energies. At the upper boundary $\Phi^-(E,z = a)$ is specified by the incident low energy auroral spectrum.

The low energy computations are started at 500 eV and work downwards taking into account energy cascading and scattering. Thus, although one can identify an initial degraded primary and secondary electron production

rate arising from ionizations caused by E > 500 eV electrons, further ionizations by E < 500 eV electrons are cumulatively computed such that the final spectrum cannot be segregated into a hierarchy of primary, tertiary, etc. electrons. The result obtained is the complete auroral energy spectrum which includes the effects of electron transport and multiple collisions.

Once the auroral electron fluxes have been found, optical emissions, ionization rates and ionospheric heating rates are obtained using the different excitation and ionization cross sections described in the preceding paragraphs.

III Results

As a first application of the present model we consider the behavior of nearly monoenergetic electrons having an isotropic pitch angle distribution in the downwards hemisphere. The results for these cases can be compared directly with the work of Rees (1969) and Rees and Maeda (1973). Following the discussion of monoenergetic electron effects, results are given for more realistic electron fluxes typical of the nighttime auroral oval and daytime polar cusp. In all examples a vertical magnetic field ($I = 90^{o}$) is assumed, and a 1000°K thermospheric model of Banks and Kockarts (1973) has been adopted.

Monoenergetic Electrons

We assume that the incident electrons are isotropic in pitch angle over the lower hemisphere at an initial height of 585 km. The energy

distribution is Gaussian and has the form

$$\varphi = A\, e^{-(E-E_o)^2/2\sigma^2} \tag{11}$$

where the value $\sigma = 0.1\, E_o$ is adopted for E_o = 0.42, 0.8, 2.0, 5.0, and 10 keV.

The normalization factor, A, for (11) has been chosen to agree with the unit incident flux normalization adopted by Rees (1963, 1969). If φ is the pitch angle dependent incident flux, the incident or, more commonly, the perpendicular flux is defined through an integration over solid angle with the factor $v \cos\theta$; i.e.

$$\Phi_{unit} = \pi\varphi\,(\text{isotropic}) \tag{12}$$

The fluxes plotted in the following figures represent hemispherical fluxes described by Equations (6) and (7) and the normalization demanded by (12) has been chosen only for the purposes of comparison with other work.

As energetic electrons penetrate the atmosphere low energy electrons in the range 0 to 500 eV are created through impact-ionization and excitation. The way in which these electrons are created has been briefly discussed in Section I. Figure 4 shows the production rates of 0 to 500 eV electrons at several altitudes for an incident E_o = 10 keV flux. Although both secondaries and degraded primaries contribute to the total production rate over this energy range, cascading hides the simple distribution of secondaries and degraded primaries sketched in Figure 1.

Computations of electron flux as a function of altitude have been made for monoenergetic spectrums characterized by values of E_o in the range 0.42 to 10 keV. Figure 5 gives the vertical variation of Φ^+ and Φ^- at several energies for E_o = 10 keV. From these results it can be seen that although there is no incident [$\Phi^-(z = 585$ km)] flux present at the lower energies, an upward (Φ^+) flux is created through elastic and inelastic scattering. As shown, this backscattered, energy degraded, flux represents an outward flow of low energy electrons from the atmosphere.

Another feature apparent in Figure 5 is the attenuation of the incident electron flux at the center energy E_o. At high altitudes these changes arise from magnetic mirroring while deeper in the atmosphere both pitch angle diffusion and energy loss are present.

Information about the energy distribution of the downcoming electron fluxes at different altitudes is contained in Figure 6. As expected from the previous work of Rees, et al.(1969), Rees (1969), Rees and Maeda (1973), Berger and Seltzer (1970) and others, the portion of the spectrum in the range 0 to 200 eV is steep, reflecting directly the way secondary electrons are produced (see Equation 4). This decline, coupled with the eventual rise in the flux when the presence of degraded primary electrons becomes important, has been discussed previously be Shemansky, et al. (1972) and Rees and Maeda (1973). Although earlier calculations (see Rees, 1969, for example) could not properly bridge this transition region, the present results and those of Rees and Maeda (1973) give consistent agreement for energies at 2 keV and above.

A second interesting feature of Figure 6 is the tendency for the low energy portion of the electron spectrum to be relatively insensitive to changes in altitude. Such a behavior can be predicted in a crude way from theory. If we neglect transport and cascading, the rate at which secondary electrons are produced is given by $n\sigma_i(E_p)\,\phi_i(E_p)$ where n is the neutral gas density, $\sigma_i(E_p)$ is the appropriate differential ionization cross section given by (4) and $\phi_i(E_p)$ is the incident ionizing flux. Likewise, the loss of secondary electrons at the energy E_s is given by $n\,\sigma_\ell(E_s)\,\phi(E_s)$ where $\sigma_\ell(E_s)$ is the cross section for electron loss at the energy E_s. If we equate production and loss we obtain the approximate formula

$$\phi(E_s) = \frac{\sigma_i(E_p)}{\sigma_\ell(E_s)}\phi_i(E_p) \tag{13}$$

which, since the neutral gas densities cancel, illustrates the altitude independence of the low energy flux. Of course, one cannot expect a simple relation like (13) to be strictly true; it only indicates the general trend of the results. However, we should also note that (13) predicts the way that $\phi(E_s)$ will depend upon the energy of the incoming flux. Since $\sigma_i(E_p)$ is approximately proportional to $E_p^{-1}\ln E_p$ for $E_p \geq 1$ keV, incident fluxes of progressively lower characteristic energy will produce proportionately greater numbers of low energy particles.

With regard to upward electron fluxes, their energy spectrums are similar to the downgoing fluxes with a more pronounced minimum. Examples

of the upward flux spectrums are shown in Figure 7 for E_o = 10 keV. In the present models there is a substantial backscattering of the incident electrons arising from collisions and magnetic mirroring. A plot of downward/upward flux ratios is given in Figure 8 for ϵ_o = 10 keV to illustrate the altitude variation of the flux ratio and the net albedo of the atmosphere to incoming electrons. The results for the low energy electrons show that although there are no incident low energy electrons (0 to 500 eV), scattering within the atmosphere acts to create an upwards flux of substantial magnitude. At low altitudes the ratio ϕ^-/ϕ^+ is greater than unity, indicating the influence of the incident high energy particles. Above 300 km, however, ϕ^+ is greater than ϕ^- as large fluxes of low energy electrons leave the atmosphere.

Plots of the ionization rates per unit incident flux for the monoenergetic electron fluxes are shown in Figure 9. The sharply peaked profiles at 2, 5 and 10 keV agree very well with those given by Rees (1969). At 0.42 and 0.8 keV, however, the influence of elastic scattering becomes important and we find our profiles are broader and peak higher altitudes than predicted by Rees.

A comparison of the ionization arising from electrons having energies less than and greater than 500 eV is shown in Figure 10. Over a broad range of altitudes about 70% of the ionization comes from the incident high energy electrons. Below 150 km, however, the ratio changes rapidly such that near and below the altitude of the peak ionization

rate, most of the ionization is caused by E < 500 eV electrons (including both degraded primaries and secondaries).

The present ionization rates can be directly compared with those computed from energy deposition curves and the assumption that 35 eV is expended for each electron-ion pair. The crosses in Figure 9 show the peak ionization rates derived from Fokker-Planck energy deposition calculations. These values show a systematic variation with incident energy, being too low at the lower energies and too high at the highest energy (10 keV). This behavior indicates the average energy needed to create electron-pairs is not constant with altitude but must depend to some extent upon the energy of the incoming electrons.

Finally, it is possible to give optical excitation rates for the monoenergetic fluxes. Figure 11 shows the computed 6300 A emission corrected for atmospheric quenching [$k = 7.25 \times 10^{-9} n(N_2) sec^{-1}$]. Scattering of the incident flux leads to a substantial upward flux which broadens the curves at high altitudes giving more emission than would be otherwise possible. Similar results are shown in Figure 12 for the 5577 Å emission of atomic oxygen.

Nighttime Aurora

To illustrate a more practical situation, model computations have been made using an incident electron flux spectrum measured during a

period of a moderate auroral activity at Fort Churchill, Canada. The results, described in further detail by Reasoner and Chappell (1973), give a reasonably typical incident auroral spectrum having a peak flux in the vicinity of 11 keV.

Using the incident flux, computations have been made of the electron flux spectrum at various heights within the atmosphere. The results for the downward fluxes are shown in Figure 13 while the computed ionization profile and several optical emissions are given in Figure 14. As was found for the monoenergetic cases, a pronounced minimum appears in the spectrums centered between .5 and 1 keV. Also, as the electrons penetrate more deeply into the atmosphere, the 11 keV peak is attenuated and shifted towards lower energies.

The influence of low energy incident particles can be seen in the ionization and optical emission profiles of Figure 14. Owing to differences in the elastic scattering cross sections for O and N_2, large changes occur in the low energy fluxes near 200 km, creating variations in the ionization rate and optical emissions. Below 200 km low energy electron transport becomes progressively more limited by collisions but above this height the electron free path soon becomes greater than the atmosphere scale height so that not only are the incident low energy electrons reflected by atmospheric collisions but also there is an outward seepage of electrons from the lower altitude regions where substantial numbers of secondary electrons are produced.

The ratio of downcoming to upgoing hemispherical fluxes is shown in Figure 15 as a function of energy. It appears that the albedo can range from 20% to 100%. However, it is necessary to remember that the upward flux is composed of energy degraded and scattered primaries as well as secondary particles.

Polar Cusp

A more complete discussion of electron precipitation effects in the polar cusp will be given in a later paper. To illustrate the general effects we have adopted an incident power-law spectrum of the form

$$\varphi = 2.34 \times 10^{9} E^{-1.73} \qquad \text{cm}^{-2}\ \text{sec}^{-1}\ \text{ster}^{-1}\ \text{eV} \qquad (14)$$

The downward flux spectrums resulting from this incident electron flux are shown for several altitudes in Figure 16. As before, as one progresses downwards a minimum appears in the spectrums centered between 250 to 700 eV. Similar results for $E > 1$ keV were obtained by Rees (1969).

The ionization profile and optical emissions corresponding to (14) are shown in Figure 17. Because (14) has been unrealistically extended to energies greater than 100 keV no peak is formed in the ionization profile. The 6300 A emission does peak, however, as a consequence of quenching by N_2.

Conclusions and Summary

The present model of auroral electron behavior provides a substantially more comprehensive description than has been previously available. The computations at energies greater than 500 eV are similar in some ways to other models. However, the resulting description of the flux as a function of energy, pitch angle and altitude is not used to compute an energy deposition rate, but rather is applied to ionization and excitation cross-sections to provide secondary and degraded primary production rates for electron energies in the range 0 - 500 eV. Using these production rates, the low energy program computes the remaining portions of the hemispherical flux spectrums in terms of upgoing and downgoing fluxes subject to various collisional processes.

The results for the 2, 5 and 10 keV monoenergetic electrons agree well with the recent values obtained by Rees and Maeda (1973). For these energies ionization deep in the atmosphere is not free to move significantly from its point of origin; i.e. although transport of secondaries and degraded primaries is still present above 200 km, it cannot greatly alter the low altitude effects.

At lower energies (1 keV and below) the effects of particle transport become important and computations based upon energy deposition become inaccurate, especially when high altitude optical emissions are included. In such cases low energy particles may arise from both collisional degradation and the presence of low energy electrons in the incident auroral spectrum.

Finally, the restriction of the present computations to hemispherical fluxes in the upwards and downwards directions could be removed using the methods of Stolarski (1972). However, until more detailed data are available describing the angular factors associated with elastic and inelastic collisions, such an approach would probably not be worth the vastly increased computational effort.

Acknowledgements

This work has greatly benefited from frequent discussions with Drs. M. H. Rees, R. S. Stolarski, W. C. Knudsen and Mr. W. E. Francis. Financial support at Lockheed was provided by the National Aeronautics and Space Administration under Contract NASw 2212 and by the Lockheed Independent Research Fund, and at the University of Michigan by the National Science Foundation under Grant GA 28690X2 and the National Aeronautics and Space Administration under Grant NGR 23-005-015.

REFERENCES

Banks, P. M., and A. F. Nagy, Concerning the influence of elastic scattering upon photoelectron transport and escape, J. Geophys. Res., 75, 1902, 1970.

Berger, M. J., S. M. Seltzer, and K. Maeda, "Energy deposition by auroral electrons in the atmosphere," J. Atmos. Terrest. Phys., 32, 1015, 1970.

Chappell, C. R., "The interaction of auroral electrons with the atmosphere, PhD Thesis, Rice University, Houston, Texas, September, 1968.

Fink, M., and A. C. Yates, "Theoretical electron scattering amplitudes and spin polarizations. Selected targets, electron energies 100 → 1500 eV," Atomic Data, 1, 385, 1970.

Fisk, J. B., "Atomic collision cross sections," Phys. Rev. 49, 167, 1936.

Green, A.E.S. and R. S. Stolarski, "Analytic models of electron impact excitation cross sections," J. Atmos. Terr. Phys., 34, 1703, 1972.

Grün, A.E., "Lumineszenz, photometrische Messungen der Energieabsorption in Strahlungsfeld von Elektronenquellen eindimensionaler Fall in Luft," Z. Naturf. 12A, 89, 1957.

International Tables for X-ray Crystallography, Vol. III, Physical and Chemical Tables, Kynoch Press, Birmingham, England (1962) p. 201.

Keiffer, L. J., Bibliography of low energy electron collision cross section data, National Bureau of Standards Misc. Pub. 289, 1967.

Lassattre, E. N., "Inelastic scattering of high energy electrons by atmospheric gases, Can. J. Chem., 47, 1733, 1969.

McDaniel, E. W., Collision Phenomena in Ionized Gases, John Wiley, New York, 1964.

Maeda, K., "Diffusion of low energy auroral electrons in the atmosphere," J. Atmos. Terrest. Phys., 27, 259, 1965.

Mott, N. F., and H. S. W. Massey, "The Theory of Atomic Collisions,"3rd ed., Oxford University Press, New York, 1965.

Nagy, A. F., and P. M. Banks, "Photoelectron fluxes in the ionosphere," J. Geophys. Res., 75, 6260,1970.

Nagy, A. F., and P. M. Banks, "Photoelectrons and related ionospheric effects," Space Res. 11, 1123, 1971.

Opal, C. B., W. K. Peterson, and E.C. Beatty, "Measurement of secondary electron spectra produced by electron impact ionization of a number of simple gases," J. Chem. Phys., 55, 4100, 1971.

Reasoner, D. L., and C. R. Chappell, "Twin payload observations of incident and backscattered auroral electrons, J. Geophys. Res., 78, 2187, 1973.

Rees, M. H., "Auroral ionization and excitation by incident energetic electrons," Planet. Space Sci., 11, 1209, 1963.

Rees, M. H., "Auroral electrons," Space Sci. Rev., 10, 413, 1969.

Rees, M. H., and K. Maeda, "Auroral electron spectra," to appear in J. Geophys. Res., 1973.

Rees, M. H., A. I. Stewart and J.C.G. Walker, "Secondary electrons in aurora," Planet. Space Sci. 17, 1969.

Schunk, R. W., and P. B. Hays, "Photoelectron energy losses to thermal electrons," Planet. Space Sci., 19, 113 1971.

Shemansky, D.E., T. M. Donahue, and E. C. Zipf, "N_2 positive and N_2^+ band systems and the energy spectra of auroral electrons," Planet. Space Sci., 20, 905, 1972.

Shyn, T. W., R. S. Stolarski, and G. R. Carignan, "Angular distribution of electrons elastically scattered from N_2", Phys. Rev. 6A, 1002 (1972).

Stadsnes, J. and B. Maehlum, "Scattering and absorption of fast electrons in the upper atmosphere, Internal Report, Norwegian Defense Research Establishment, Kjeller, Norway, 1965.

Stolarski, R. S.,"Calculation of Auroral Emission Rates and Heating Effects," Planet. Space Sci., 16, 1265, 1968.

Stolarski, R. S., "Analytic approach to photoelectron transport," J. Geophys. Res., 16, 2862, 1972.

Sunshine, G., B. B. Aubrey, and B. Bederson, "Absolute measurements of total cross sections for the scattering of low-energy electrons by atomic and molecular oxygen," Phys. Rev., 154, 1, 1967.

Walt, M., W. M. MacDonald, and W. E. Francis, "Penetration of auroral electrons into the atmosphere," in Physics of the Magnetosphere, ed. R. L. Carovillano, Reidel, Dordrecht, 1968.

FIGURE CAPTIONS

1. Schematic diagram of the energy distribution of primary and secondary electrons created through impact ionization.

2. Electron production rates as a function of energy in the range 0 to 500 eV at various altitudes for the nighttime auroral spectrum discussed in Section III.

3. A comparison of discrete (solid curve) and continuous (dashed curve) energy loss rates for N_2. The discrete losses include ionization and excitation while the continuous loss is based upon the Bethe formula of equation (3).

4. Electron production rates as a function of energy in the range 0 to 500 eV for a 10 keV Gaussian (monoenergetic) incident spectrum. The rates are normalized to unity incident (perpendicular) flux.

5. Vertical profiles of downward and upward electron fluxes at selected energies for an incident Gaussian (monoenergetic) flux of 10 keV normalized to unity incident (perpendicular flux).

6. Downward hemispherical fluxes at various altitudes for various Gaussian (monoenergetic) incident spectrums lying between 0.42 and 10 keV. The fluxes are normalized to unity incident (perpendicular) flux.

7. Upward hemispherical fluxes at various altitudes for a 10 keV Gaussian (monoenergetic) incident spectrum.

8. Ratio of Φ^-/Φ^+ for 10 keV Gaussian (monoenergetic) incident electrons as a function of energy at several altitudes. Values less than 1 show where the upward flux is greater than the downward flux.

9. Ionization rates per unit incident (perpendicular) flux for Gaussian (monoenergetic) fluxes in the range 0.42 to 10 keV. The symbol ⊗ indicates the results of energy deposition and the assumption that 35 eV is expended for each electron-ion pair.

10. Comparison of ionization produced by E < 500 eV electrons to the total ionization rate for different incident Gaussian (monoenergetic) fluxes.

11. 6300 Å emission profiles (with quenching) for incident Gaussian (monoenergetic) spectrums normalized to unity incident (perpendicular) flux.

12. 5577 Å emission profiles for atomic oxygen with incident Gaussian (monoenergetic) spectrums normalized to unity incident (perpendicular) flux.

13. Downward flux spectrums for a nighttime auroral spectrum obtained from rocket measurements by Reasoner and Chappell (1973). For this example the hemispherical flux has been divided by 2π steradians.

14. Optical emissions and the ionization profile associated with the incident nighttime auroral spectrum of Figure 13.

15. Ratio of Φ^-/Φ^+ as a function of energy at several altitudes for the nighttime auroral spectrum shown in Figure 13.

16. Downward flux spectrums for a power law incident spectrum typical of the polar cusp. For this example the hemispherical flux has been divided by 2π steradians.

17. Optical emissions and the ionization profile arising from the polar cusp type incident spectrum shown in Figure 16.

TABLE 1

MEAN ELECTRON EXCITATION PARAMETER, I

	I(eV)
N_2	80.5
O_2	92.0
O	92.0

TABLE 2

SECONDARY ELECTRON ENERGY DEGRADATION COEFFICIENT

	$\tilde{E}$(eV)
N_2	14.1
O_2	18.9
O	15.0

TABLE 3

ADOPTED TOTAL ELECTRON IONIZATION CROSS SECTION PARAMETERS

	I	A	Ω	ν	p	ν
N_2	19.96	1.1	0.85	1	1.2	2
O_2	18.5	1.2	0.87	1	1.1	3
O	16.1	0.84	0.85	0.3	1.2	1

TABLE 4

ELECTRON IMPACT

IONIZATION CROSS SECTION PARAMETERS

	State	I	A	Ω	ν	γ	p
N_2	$X^2\Sigma_g^+$	15.58	0.370	0.80	3.0	1.0	1.2
	$A^2\pi_u$	16.73	0.160	0.83	1.0	1.0	1.2
	$B^2\Sigma_u^+$	18.75	0.073	0.83	2.0	1.0	1.2
	$D^2\pi_g$	22.0	0.056	0.83	2.0	1.0	1.2
	$C^2\Sigma_u^+$	23.6	0.060	0.83	2.0	1.0	1.2
	Dissociative	25.0	0.380	0.96	2.0	1.0	1.2
O_2	$X^2\pi_g$	12.1	0.058	0.80	2.0	1.0	1.1
	$a^4\pi_u$	16.1	0.150	0.80	2.0	1.0	1.1
	$A^2\pi_u$	16.9	0.150	0.80	2.0	1.0	1.1
	$b^4\Sigma_g^-$	18.2	0.130	0.80	2.0	1.0	1.1
	B	23.0	0.064	0.80	2.0	1.0	1.0
	Diss.($O^{+4}S$)	18.0	0.400	0.93	3.0	1.0	1.1
	Diss.($O^{+2}D$)	22.0	0.250	0.93	3.0	1.0	1.0
O	^4S	13.6	0.290	0.85	1.0	0.3	1.2
	^2D	16.9	0.360	0.85	1.0	0.3	1.2
	^2P	18.5	0.190	0.85	1.0	0.3	1.2

TABLE 5

ELECTRON IMPACT EXCITATION CROSS SECTION PARAMETERS

	State	W (eV)	A_o	Ω	ν	γ
N_2	$A^3\Sigma^+_u$	6.14	0.226	3.0	1.0	1.0
	$B^3\pi_g$	7.30	0.178	3.0	1.0	3.0
	$C^3\pi_u$	11.03	0.28	3.0	1.0	3.0
	$a^1\pi_g$	9.10	0.136	1.0	1.0	1.0
	$b^1\pi_u$	12.85	0.67	0.75	3	1.0
	$b^1\Sigma^+_u$	14.0	0.33	0.75	3	1.0
	Σ Rydberg	13.75	2.66	0.75	3	1.0
	vib W = 10	1.4	1.5×10^5	16	9	1.0
O_2	$a^1\Delta_g$	0.98	0.0005	3.0	1.0	3.0
	$b^1\Sigma^+_g$	1.64	0.0005	3.0	1.0	3.0
	$A^3\Sigma^+_u$	4.5	0.021	0.9	1.0	3.0
	$B^3\Sigma^-_u$	8.4	0.23	0.75	2.0	1.0
	9.9 eV Allowed	9.9	0.08	0.75	3.0	1.0
	Σ Rydberg	13.5	2.77	0.75	3.0	1.0
	vib	.25	9.57×10^{-4}	.90	1.0	1.0
O	^1D	1.96	0.01	1.0	2.0	1.0
	^1S	4.17	0.0042	1.0	1.0	0.5
	^3S	9.53	0.0465	1.0	1.0	0.5
	^5S	9.15	0.023	2.0	1.0	1.0
	$\Sigma(\Delta l=1, \Delta s=0)$	14.2	0.367	0.75	3.0	1.0
	$\Sigma(\Delta s=1)$	14.7	0.694	2.0	1.0	1.0
	$\Sigma(\Delta l=0, \Delta s=0)$	13.5	0.043	0.75	1.0	2.0

TABLE 6

ADOPTED ELASTIC SCATTERING CROSS SECTIONS (10^{-16} cm^2)

Electron Energy (eV)	N_2	O_2	O
100	8.1	8.1	4.9
150	7.2	7.2	4.4
200	6.3	6.3	3.8
250	5.5	5.5	3.3
300	4.7	4.7	2.9
400	3.5	3.5	2.1
500	2.4	2.4	1.4

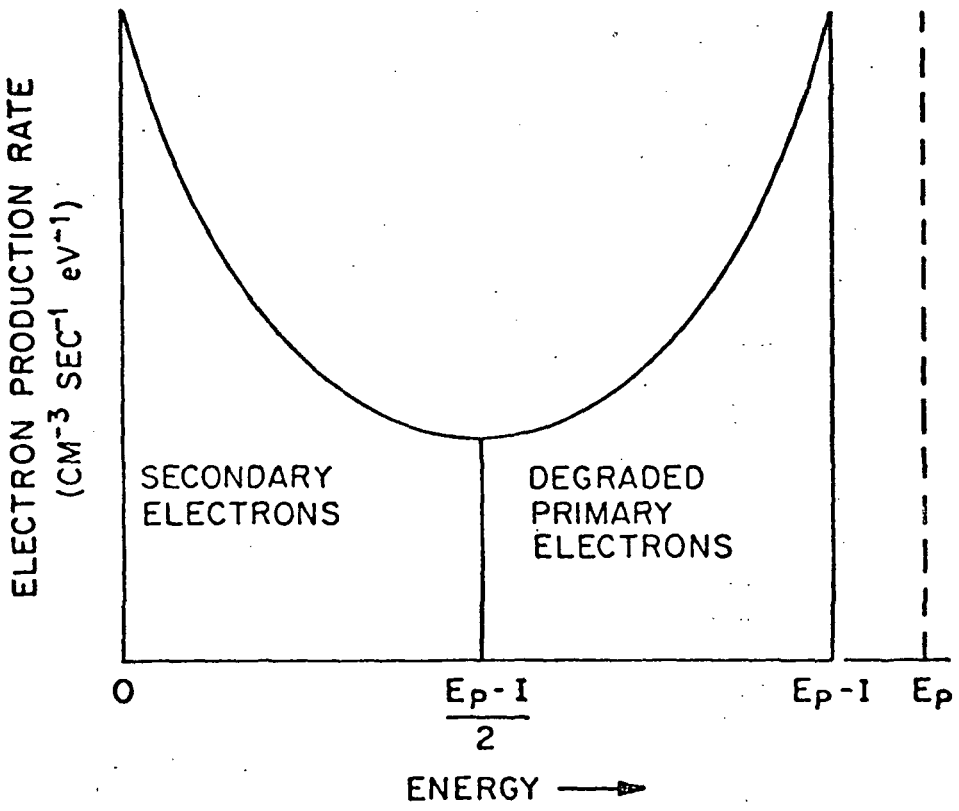
ELECTRON PRODUCTION RATE
(CM^{-3} SEC^{-1} eV^{-1})
SECONDARY
ELECTRONS
DEGRADED
PRIMARY
ELECTRONS
0
$\frac{E_p - I}{2}$
$E_p - I$
E_p
ENERGY

Figure 1

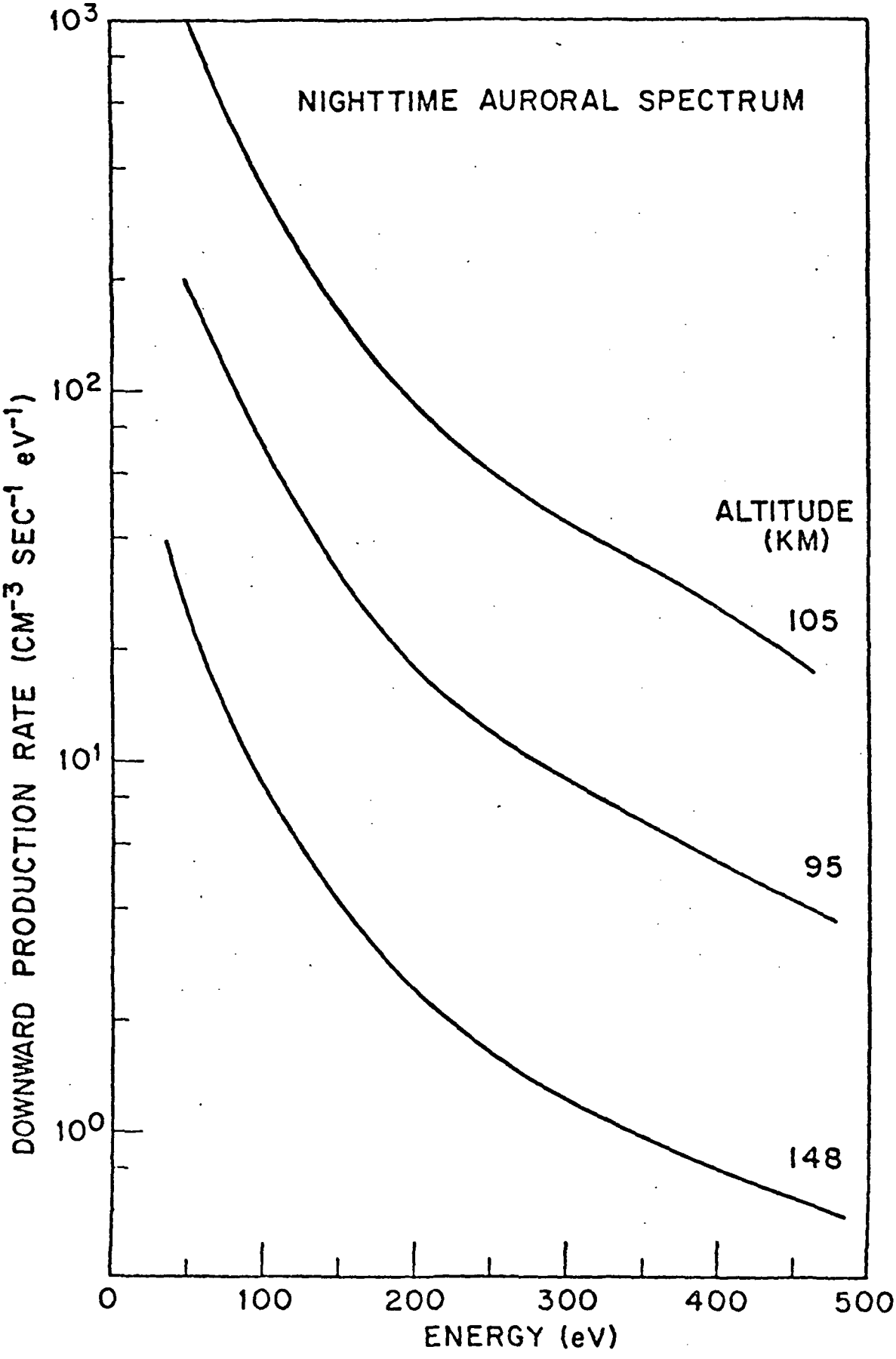
NIGHTTIME AURORAL SPECTRUM
DOWNWARD PRODUCTION RATE (CM^{-3} SEC^{-1} eV^{-1})
10^3
10^2
10^1
10^0
ALTITUDE (KM)
105
95
148
0
100
200
300
400
500
ENERGY (eV)

Figure 2

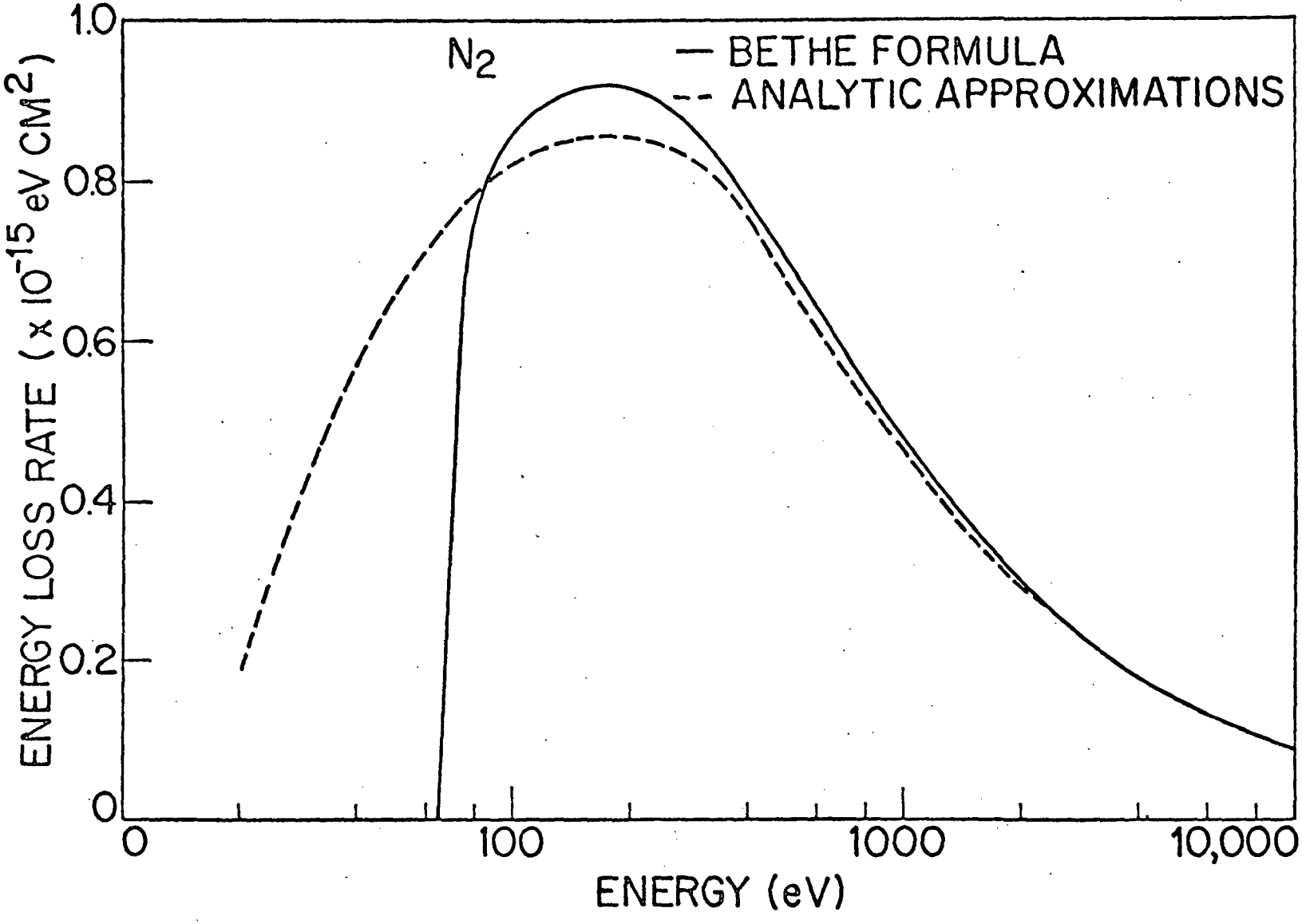
N_2
— BETHE FORMULA
-- ANALYTIC APPROXIMATIONS
ENERGY LOSS RATE ($\times 10^{-15}$ eV CM^2)
1.0
0.8
0.6
0.4
0.2
0
0
100
1000
10,000
ENERGY (eV)

Figure 3

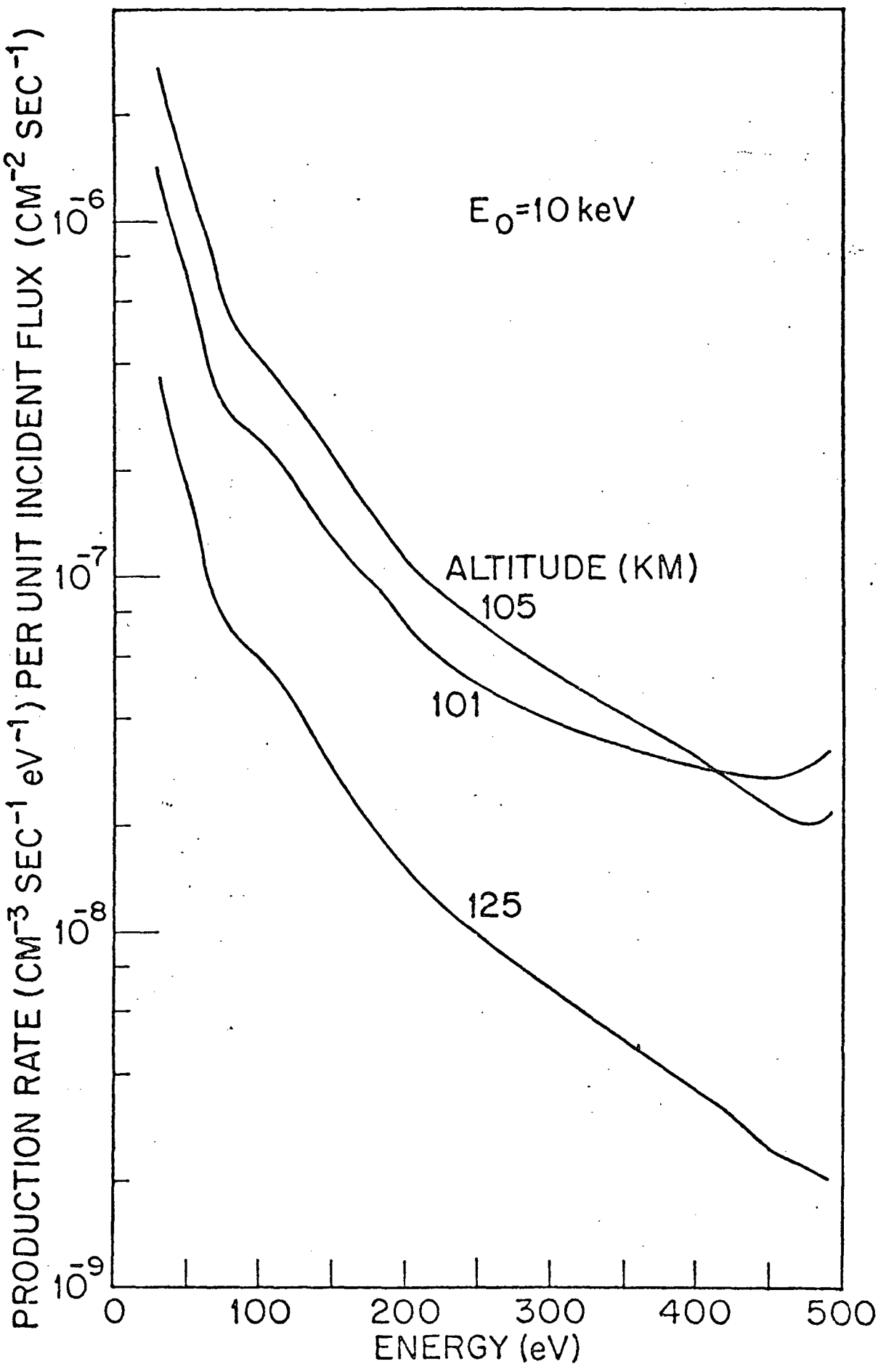
PRODUCTION RATE (CM^{-3} SEC^{-1} eV^{-1}) PER UNIT INCIDENT FLUX (CM^{-2} SEC^{-1})
E_0=10 keV
ALTITUDE (KM)
105
101
125
10^{-6}
10^{-7}
10^{-8}
10^{-9}
0
100
200
300
400
500
ENERGY (eV)

Figure 4

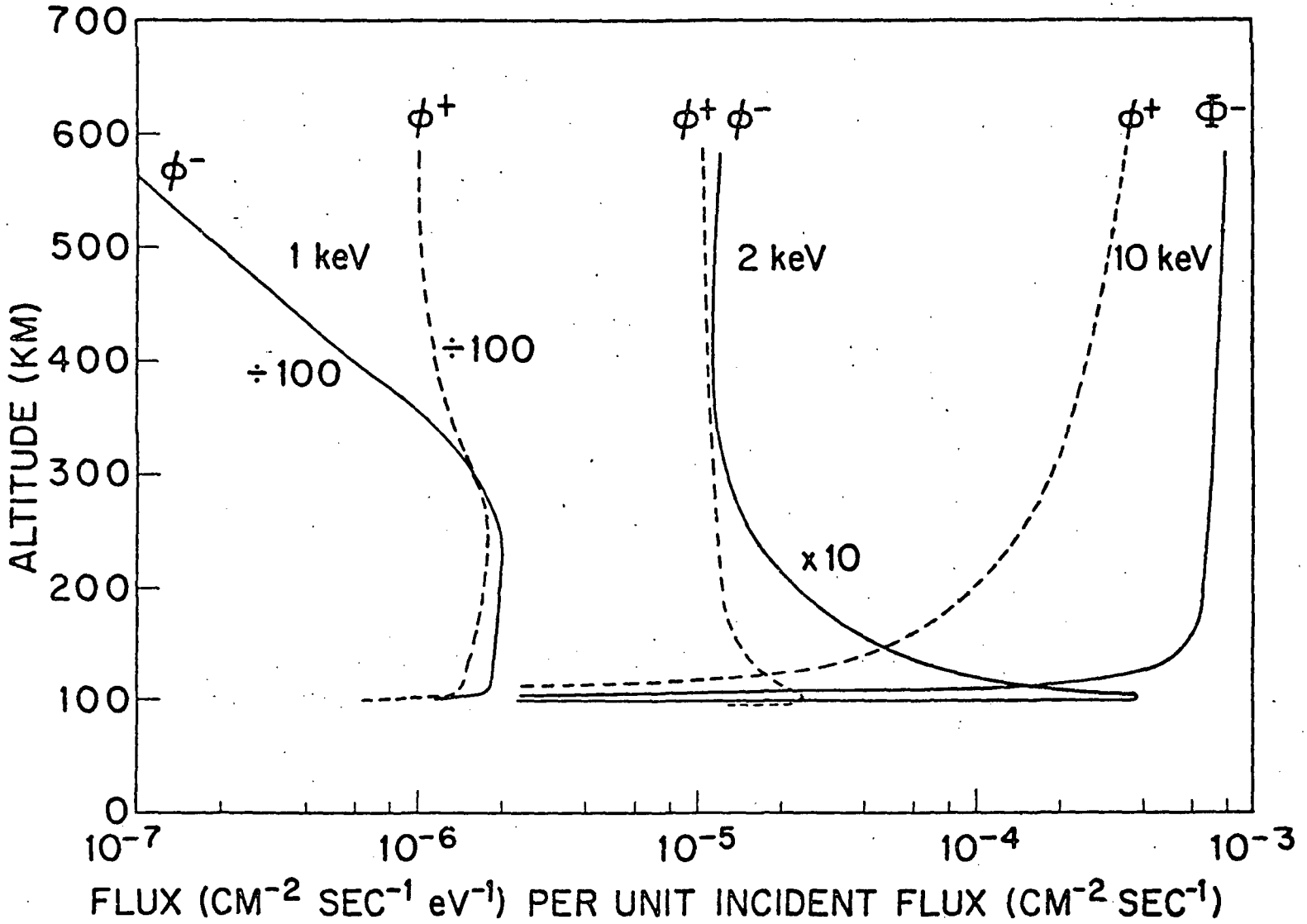
700
600
500
400
300
200
100
0
ALTITUDE (KM)
ϕ^-
1 keV
÷100
ϕ^+
÷100
ϕ^+ ϕ^-
2 keV
x10
ϕ^+ Φ^-
10 keV
10^{-7}
10^{-6}
10^{-5}
10^{-4}
10^{-3}
FLUX (CM^{-2} SEC^{-1} eV^{-1}) PER UNIT INCIDENT FLUX (CM^{-2} SEC^{-1})

Figure 5

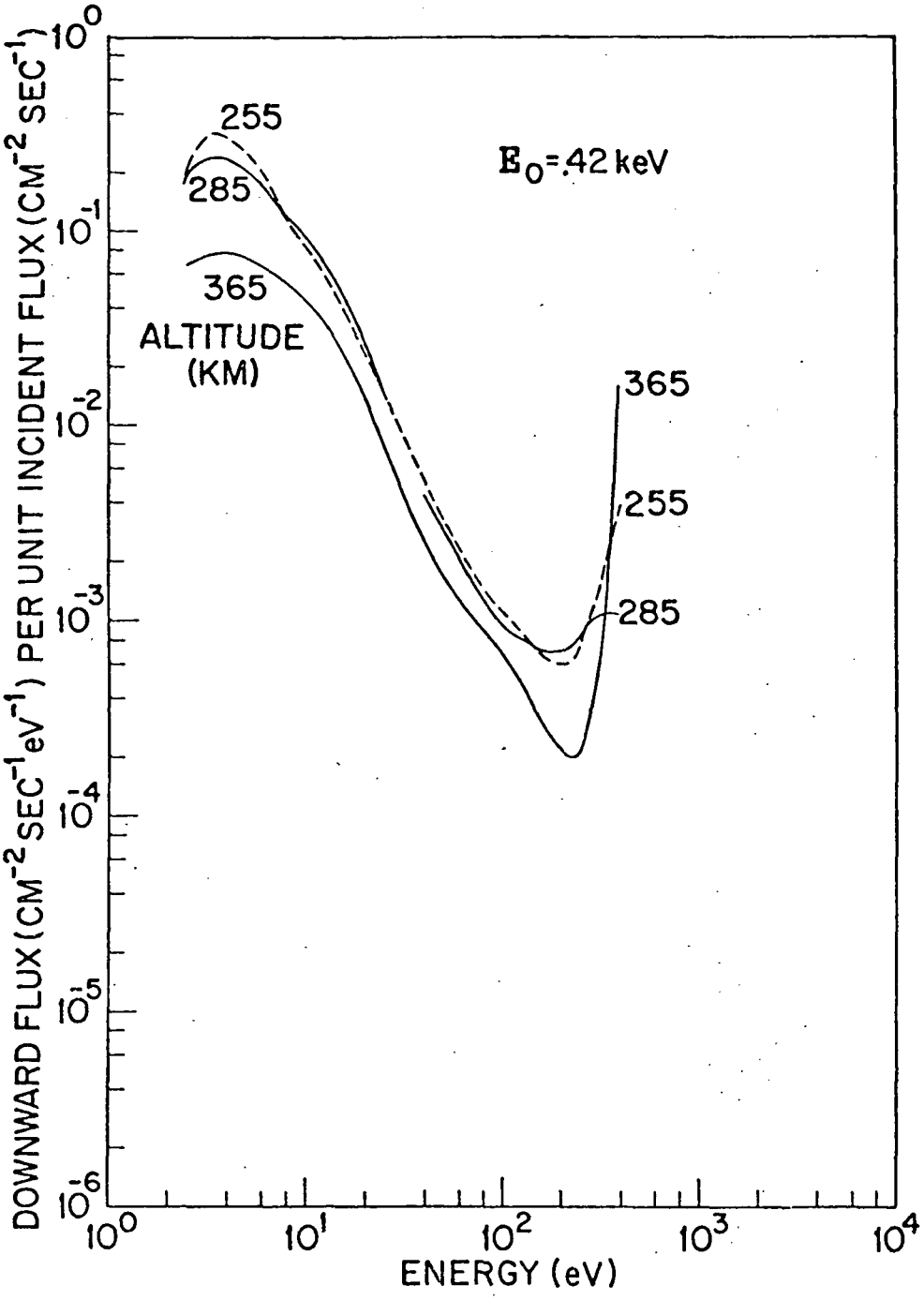
DOWNWARD FLUX (CM^{-2} SEC^{-1} eV^{-1}) PER UNIT INCIDENT FLUX (CM^{-2} SEC^{-1})
ENERGY (eV)
E_0=.42 keV
255
285
365
ALTITUDE (KM)
365
255
285
10^0
10^{-1}
10^{-2}
10^{-3}
10^{-4}
10^{-5}
10^{-6}
10^0
10^1
10^2
10^3
10^4

Figure 6a

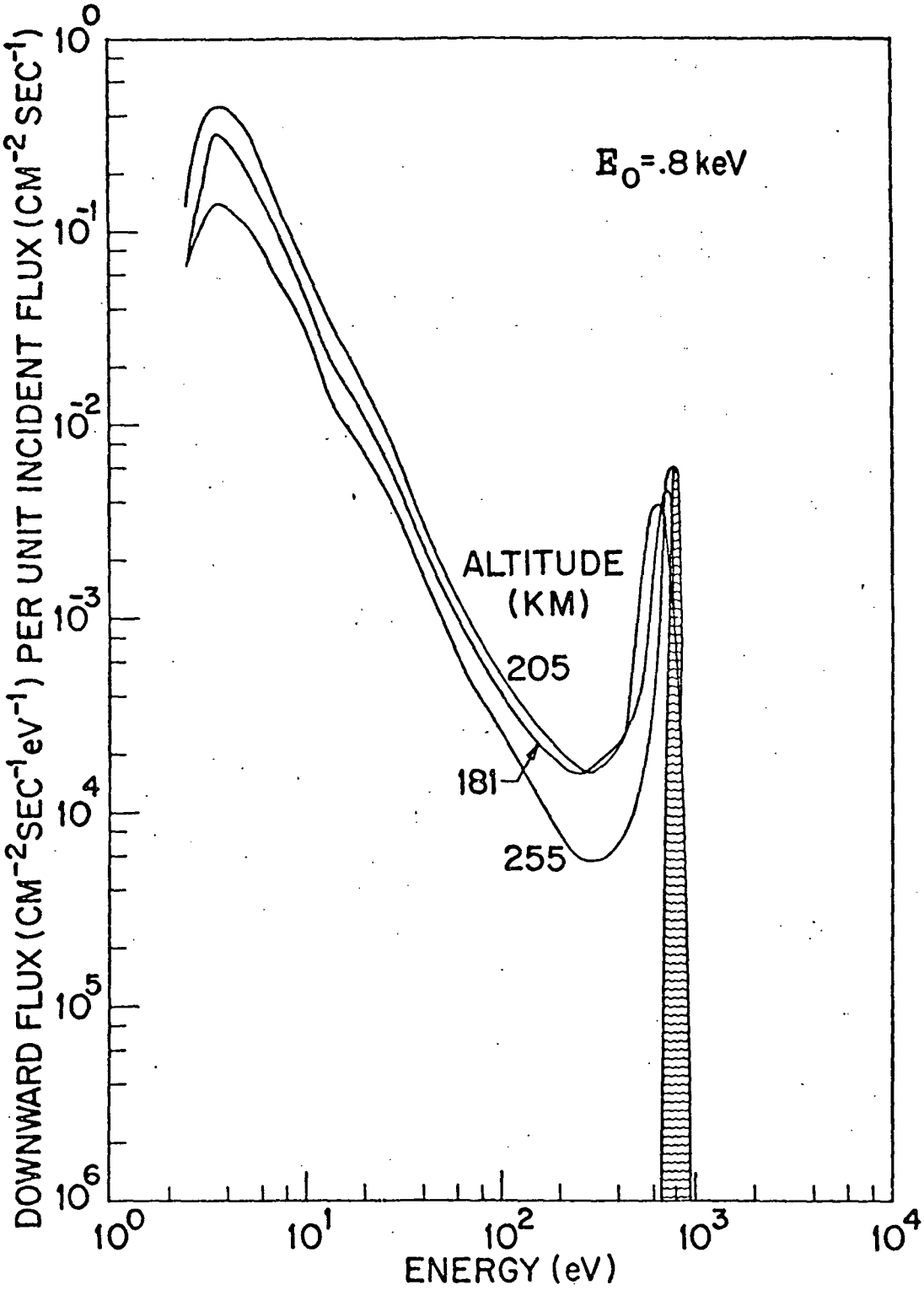
DOWNWARD FLUX (CM^{-2}SEC^{-1}eV^{-1}) PER UNIT INCIDENT FLUX (CM^{-2} SEC^{-1})
10^0
10^{-1}
10^{-2}
10^{-3}
10^{-4}
10^{-5}
10^{-6}
E_0=.8 keV
ALTITUDE
(KM)
205
181
255
10^0
10^1
10^2
10^3
10^4
ENERGY (eV)

Figure 6b

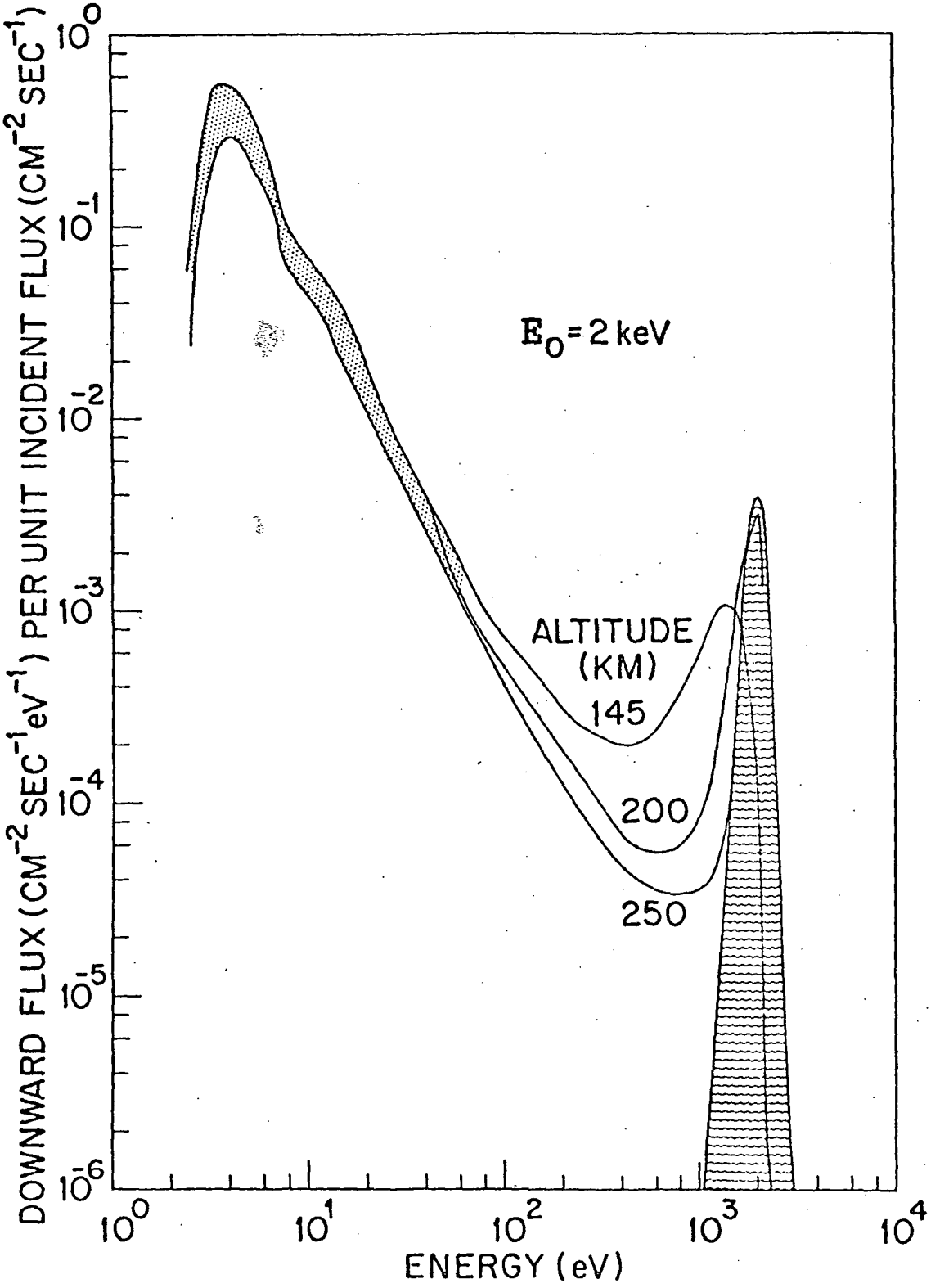
DOWNWARD FLUX (CM^{-2} SEC^{-1} eV^{-1}) PER UNIT INCIDENT FLUX (CM^{-2} SEC^{-1})
10^{0}
10^{-1}
10^{-2}
10^{-3}
10^{-4}
10^{-5}
10^{-6}
E_0 = 2 keV
ALTITUDE (KM)
145
200
250
10^{0}
10^{1}
10^{2}
10^{3}
10^{4}
ENERGY (eV)

Figure 6c

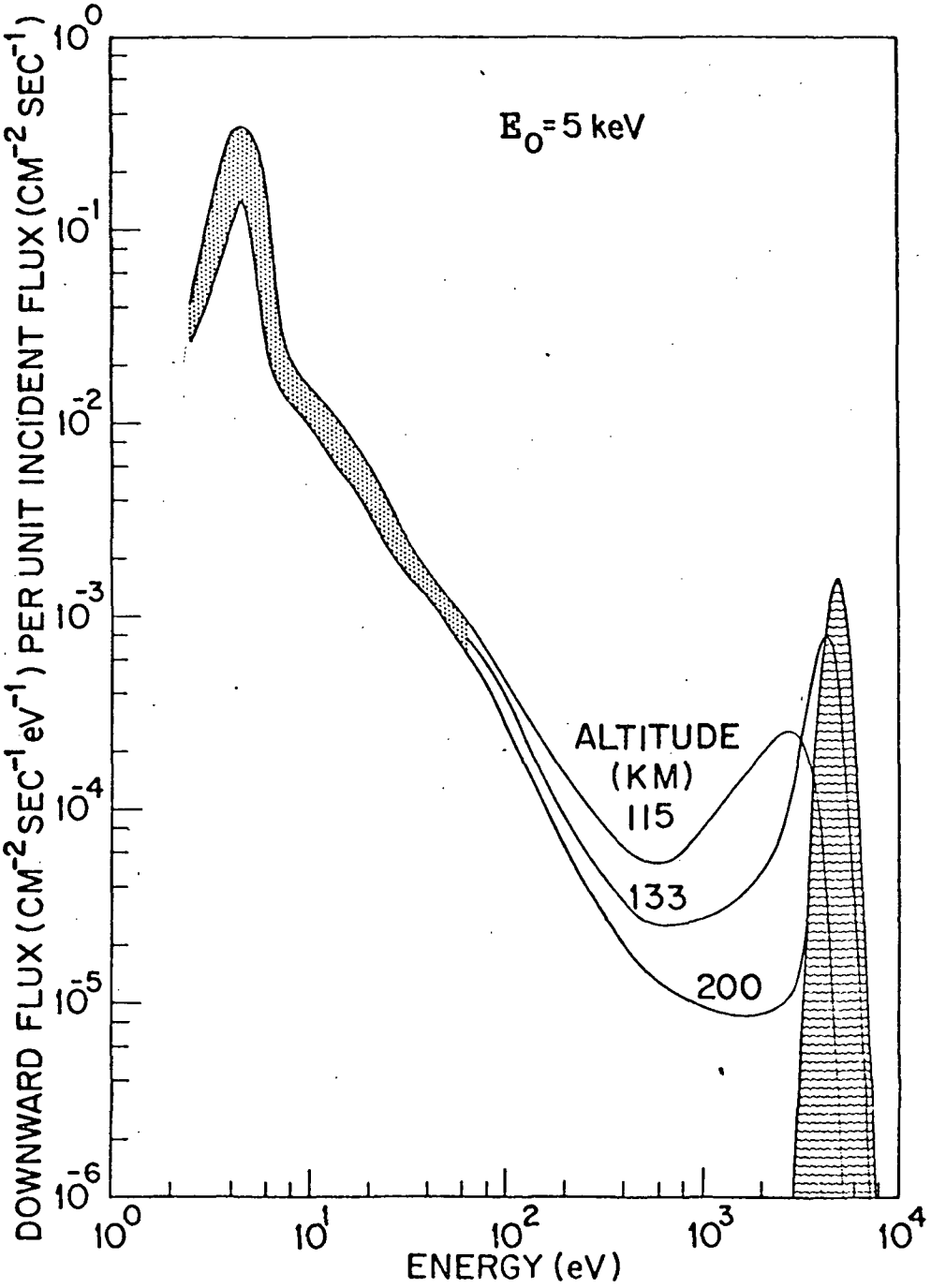
E_0=5 keV
ALTITUDE
(KM)
115
133
200
DOWNWARD FLUX ($CM^{-2}SEC^{-1}eV^{-1}$) PER UNIT INCIDENT FLUX ($CM^{-2}SEC^{-1}$)
ENERGY (eV)
10^0
10^{-1}
10^{-2}
10^{-3}
10^{-4}
10^{-5}
10^{-6}
10^0
10^1
10^2
10^3
10^4

Figure 6d

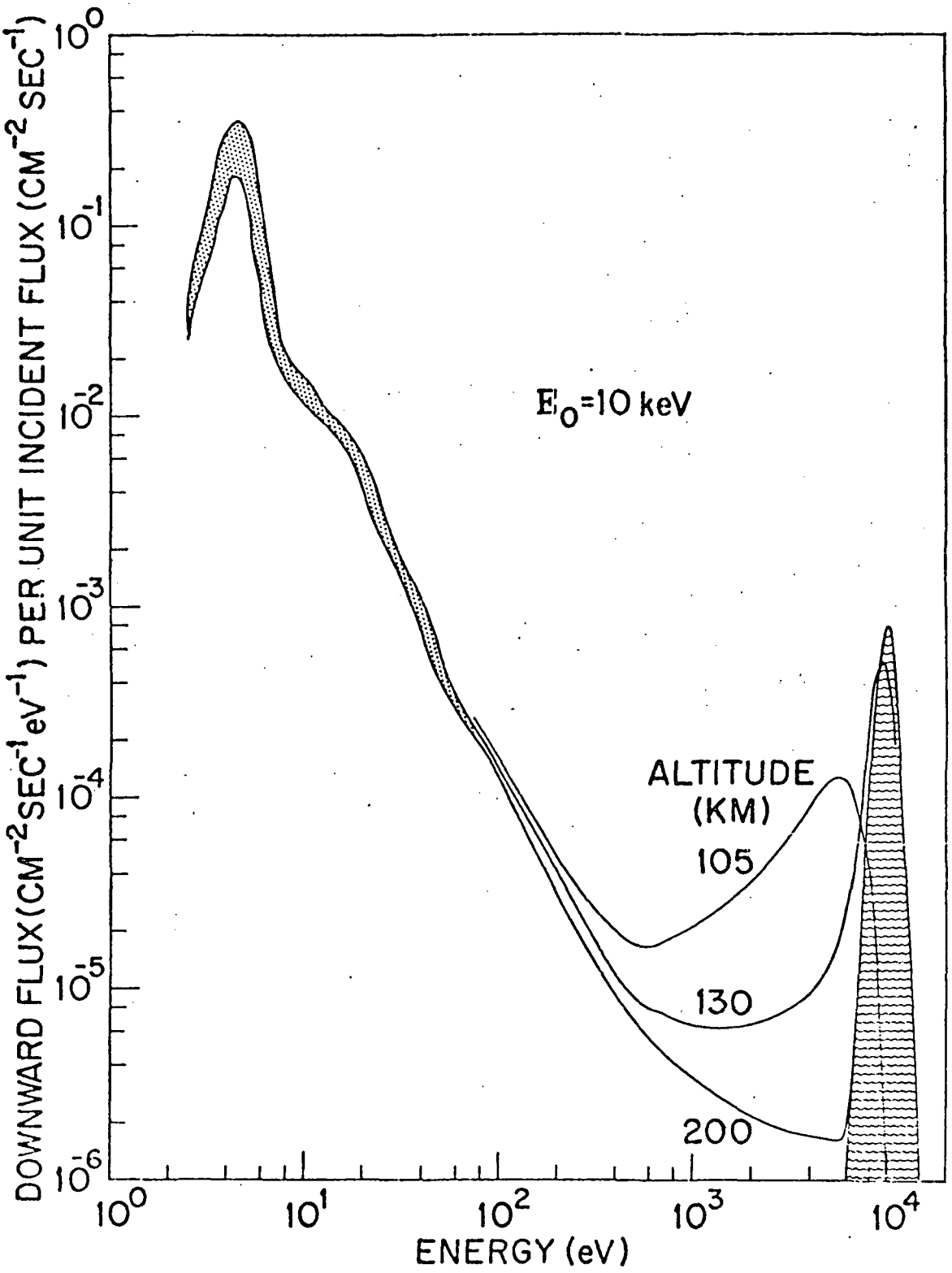
DOWNWARD FLUX (CM^{-2}SEC^{-1}eV^{-1}) PER UNIT INCIDENT FLUX (CM^{-2} SEC^{-1})
10^0
10^{-1}
10^{-2}
10^{-3}
10^{-4}
10^{-5}
10^{-6}
E_0=10 keV
ALTITUDE (KM)
105
130
200
10^0
10^1
10^2
10^3
10^4
ENERGY (eV)

Figure 6e

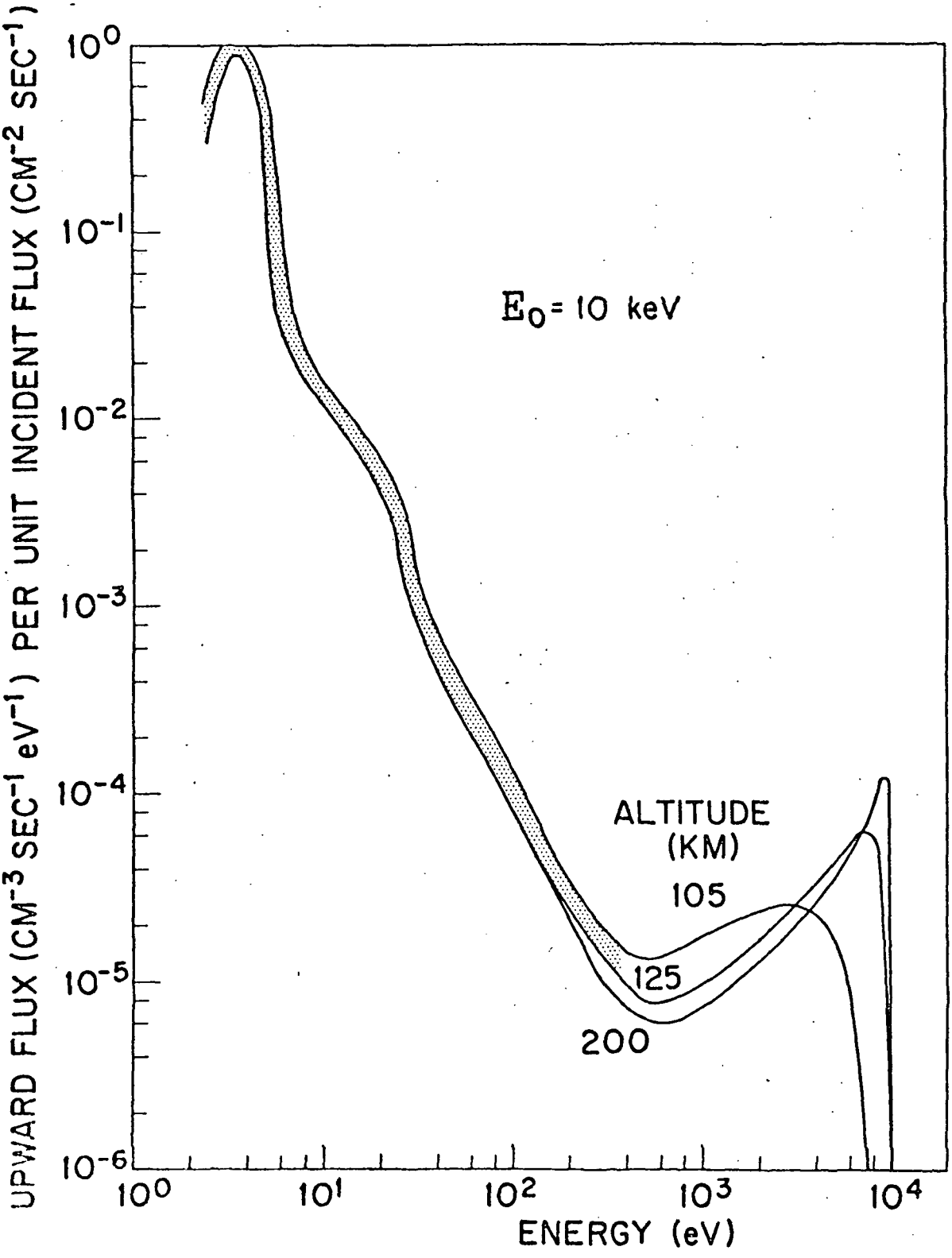
UPWARD FLUX (CM^{-3} SEC^{-1} eV^{-1}) PER UNIT INCIDENT FLUX (CM^{-2} SEC^{-1})
10^{0}
10^{-1}
10^{-2}
10^{-3}
10^{-4}
10^{-5}
10^{-6}
E_0 = 10 keV
ALTITUDE (KM)
105
125
200
10^{0}
10^{1}
10^{2}
10^{3}
10^{4}
ENERGY (eV)

Figure 7

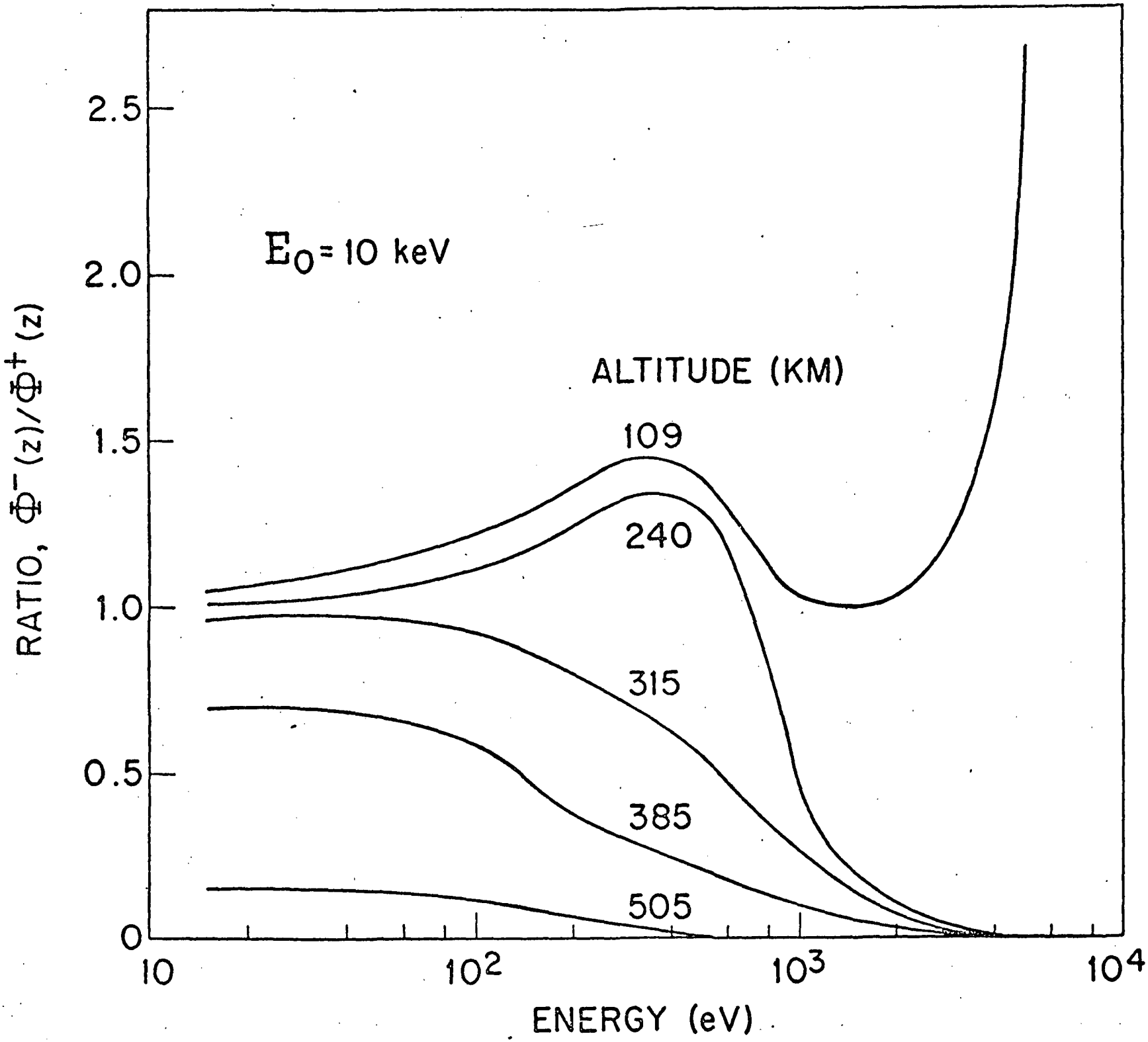
E_0 = 10 keV
ALTITUDE (KM)
109
240
315
385
505
RATIO, $\Phi^-(z)/\Phi^+(z)$
ENERGY (eV)
2.5
2.0
1.5
1.0
0.5
0
10
10^2
10^3
10^4

Figure 8

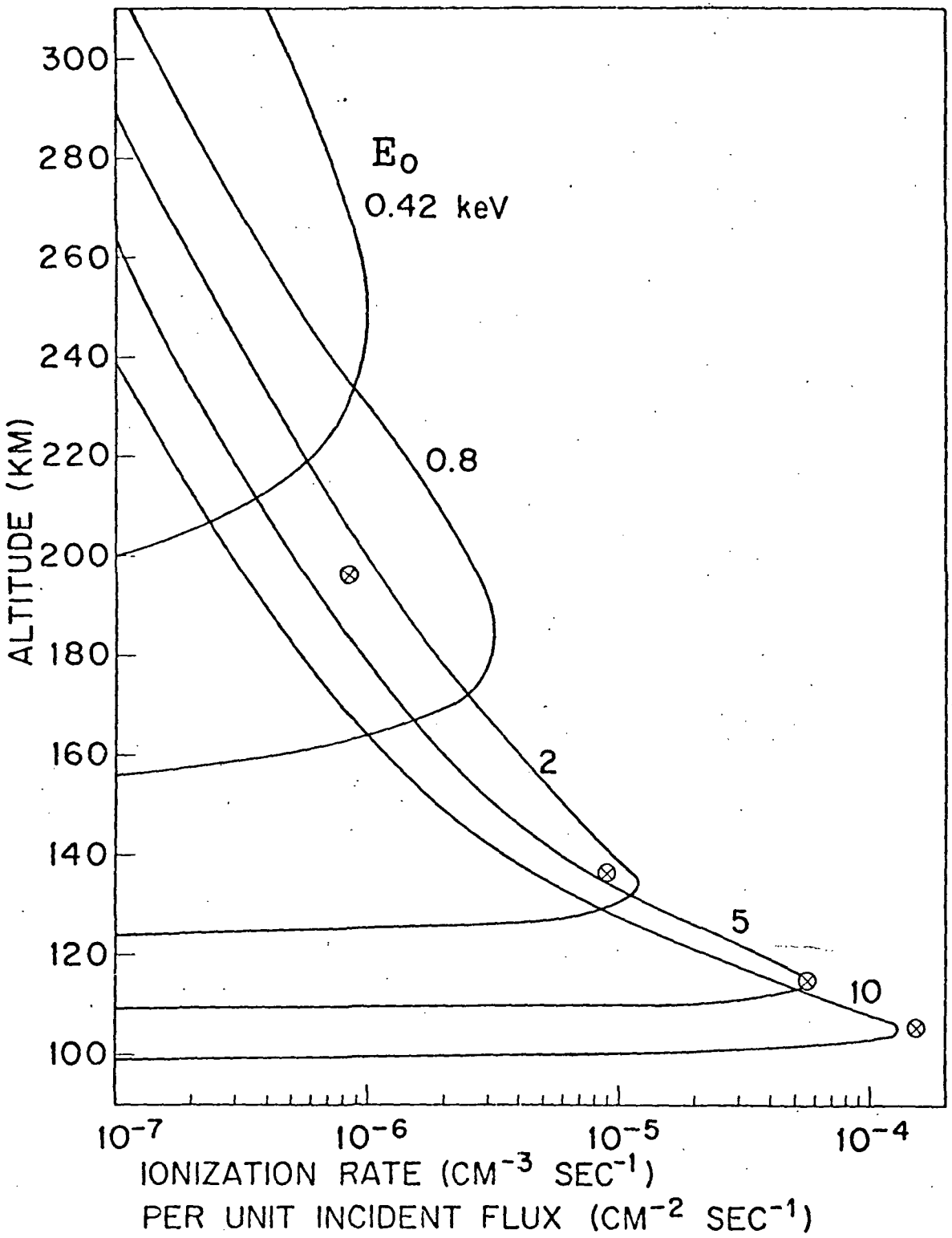
300
280
260
240
220
200
180
160
140
120
100
ALTITUDE (KM)
E_0
0.42 keV
0.8
2
5
10
10^{-7}
10^{-6}
10^{-5}
10^{-4}
IONIZATION RATE (CM^{-3} SEC^{-1})
PER UNIT INCIDENT FLUX (CM^{-2} SEC^{-1})

Figure 9

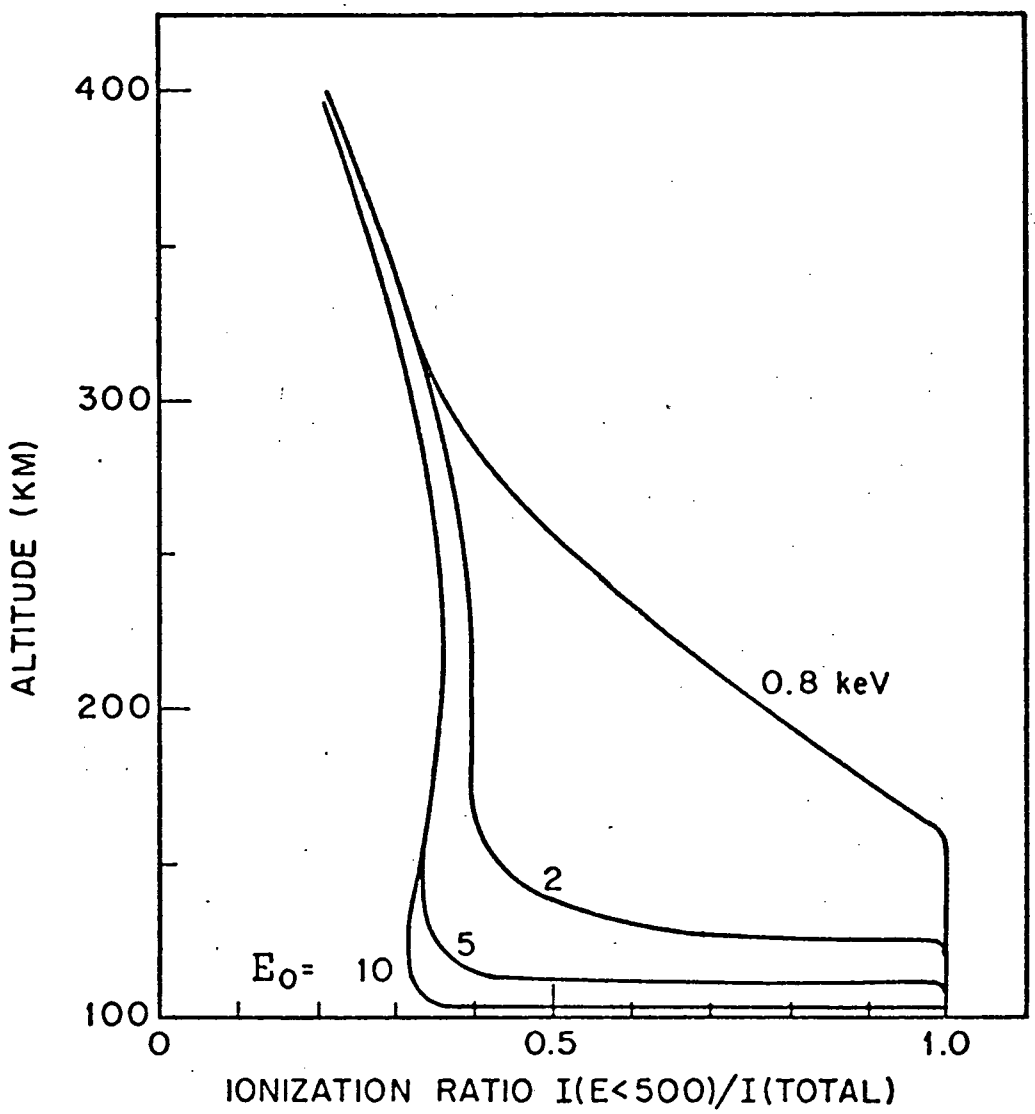
400
300
200
100
ALTITUDE (KM)
0.8 keV
2
5
10
E_0=
0
0.5
1.0
IONIZATION RATIO I(E<500)/I(TOTAL)

Figure 10

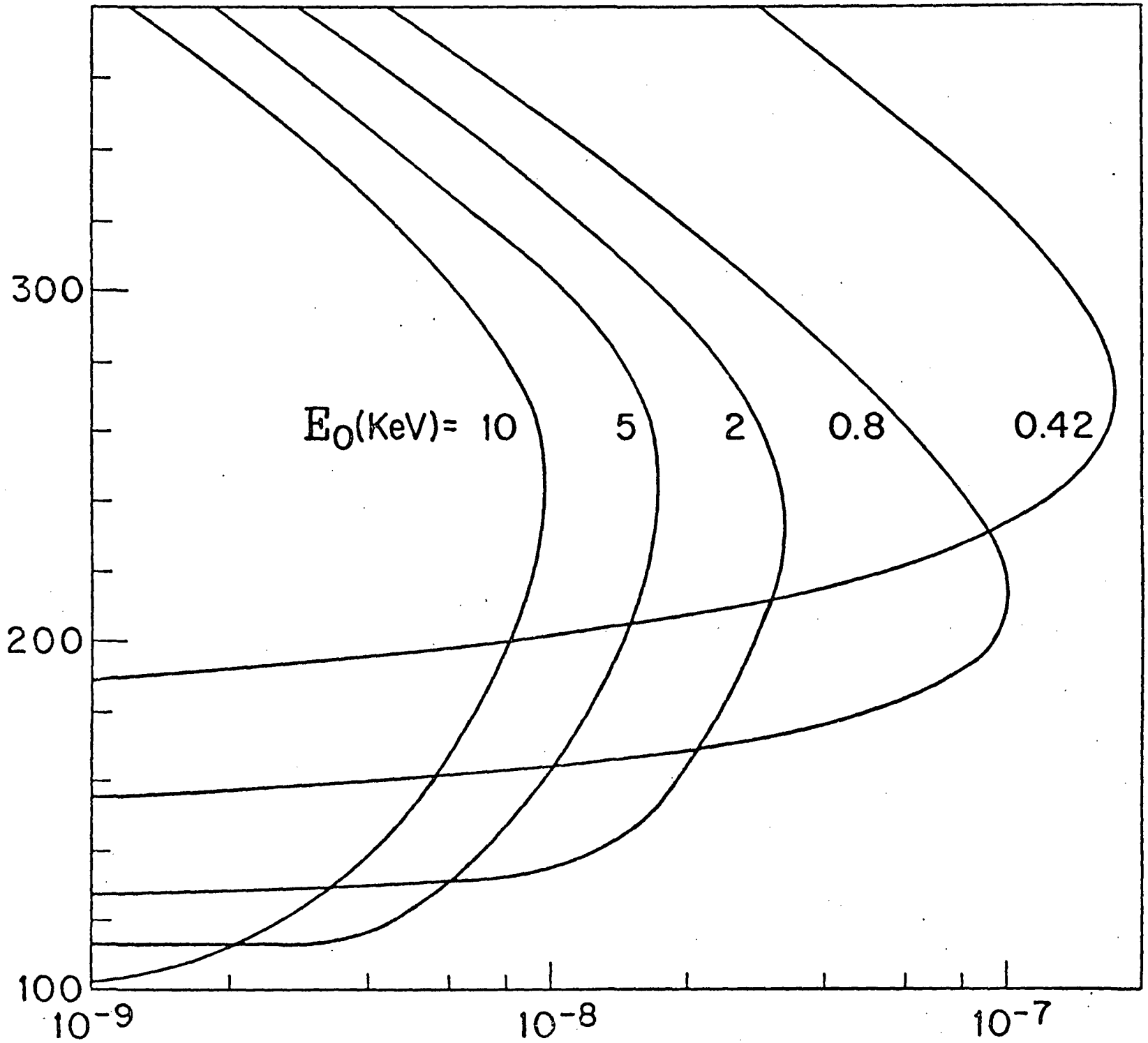
ALTITUDE (KM)
300
200
100
E_0(KeV)= 10
5
2
0.8
0.42
10^{-9}
10^{-8}
10^{-7}
6300Å EMISSION RATE ($CM^{-3}SEC^{-1}$) PER UNIT INCIDENT FLUX

Figure 11

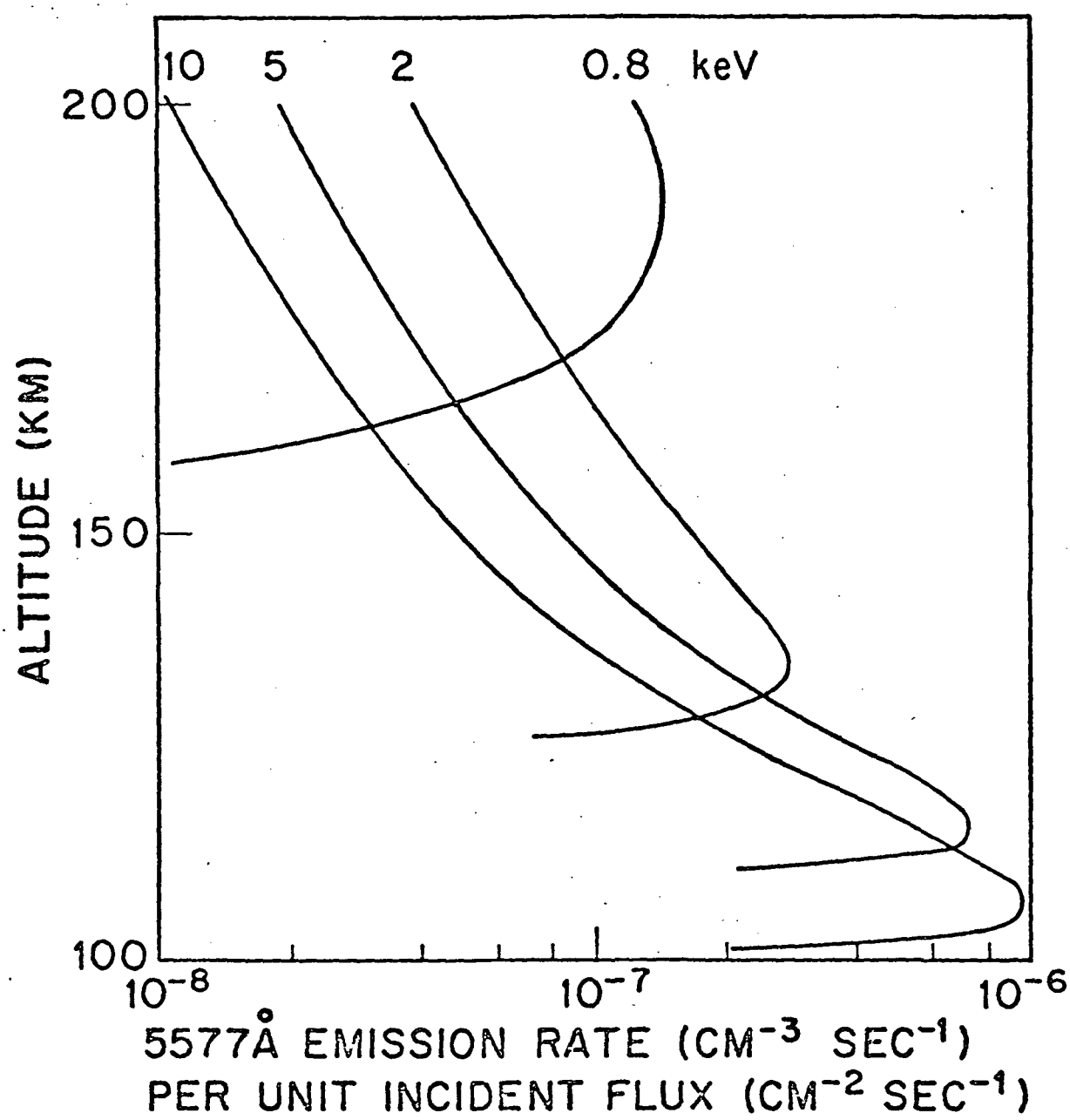
10
5
2
0.8 keV
200
150
100
ALTITUDE (KM)
10^-8
10^-7
10^-6
5577Å EMISSION RATE (CM^-3 SEC^-1)
PER UNIT INCIDENT FLUX (CM^-2 SEC^-1)

Figure 12

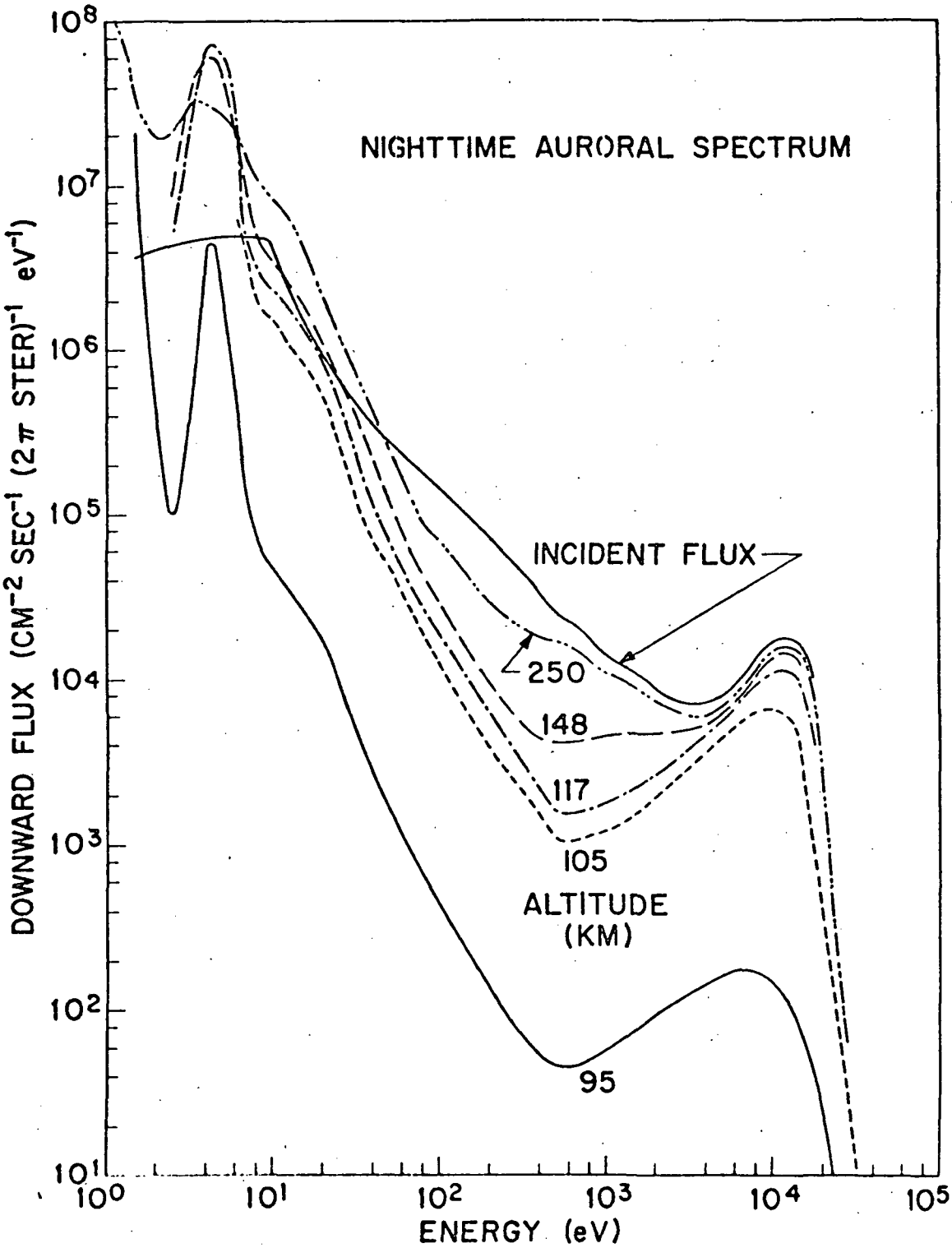
NIGHTTIME AURORAL SPECTRUM
DOWNWARD FLUX (CM⁻² SEC⁻¹ (2π STER)⁻¹ eV⁻¹)
ENERGY (eV)
INCIDENT FLUX
250
148
117
105
ALTITUDE (KM)
95
10⁸
10⁷
10⁶
10⁵
10⁴
10³
10²
10¹
10⁰
10¹
10²
10³
10⁴
10⁵

Figure 13

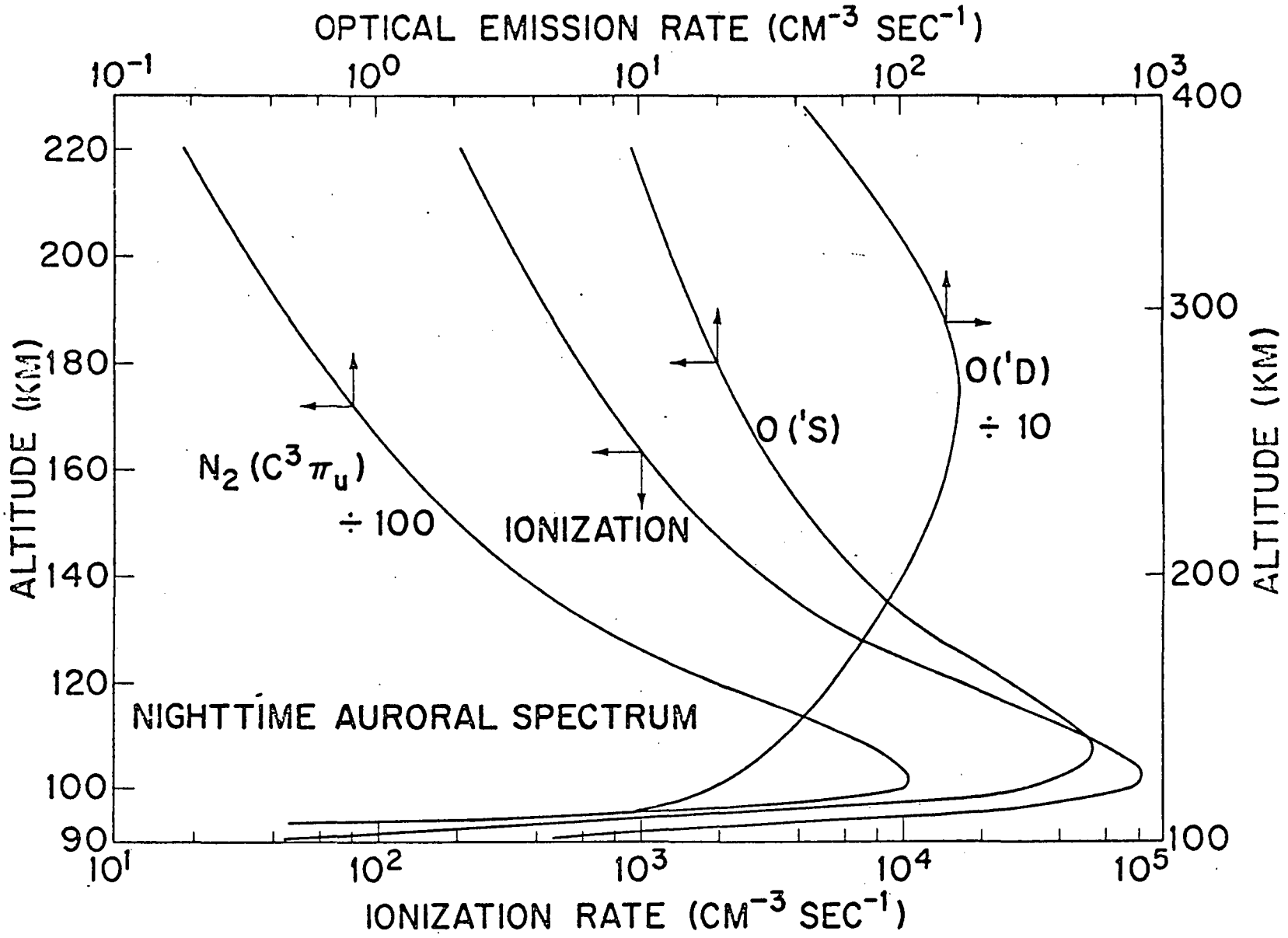
OPTICAL EMISSION RATE (CM^{-3} SEC^{-1})
10^{-1}
10^{0}
10^{1}
10^{2}
10^{3}
220
200
180
160
140
120
100
90
ALTITUDE (KM)
400
300
200
100
ALTITUDE (KM)
N_2 ($C^3\pi_u$)
÷ 100
IONIZATION
O ('S)
O ('D)
÷ 10
NIGHTTIME AURORAL SPECTRUM
10^{1}
10^{2}
10^{3}
10^{4}
10^{5}
IONIZATION RATE (CM^{-3} SEC^{-1})

Figure 14

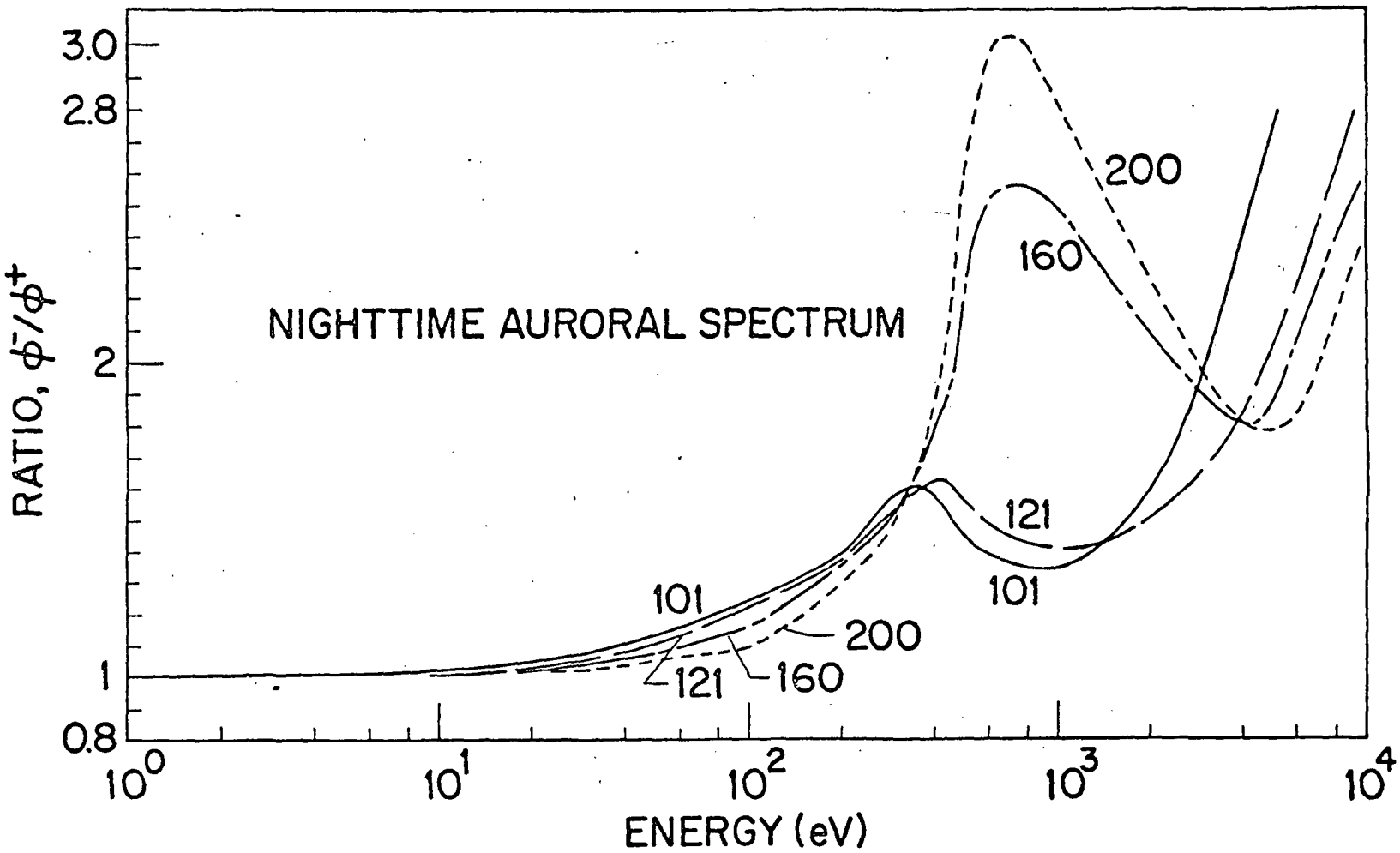
NIGHTTIME AURORAL SPECTRUM
RATIO, ϕ^-/ϕ^+
3.0
2.8
2
1
0.8
10^0
10^1
10^2
10^3
10^4
ENERGY (eV)
200
160
121
101
101
200
121
160

Figure 15

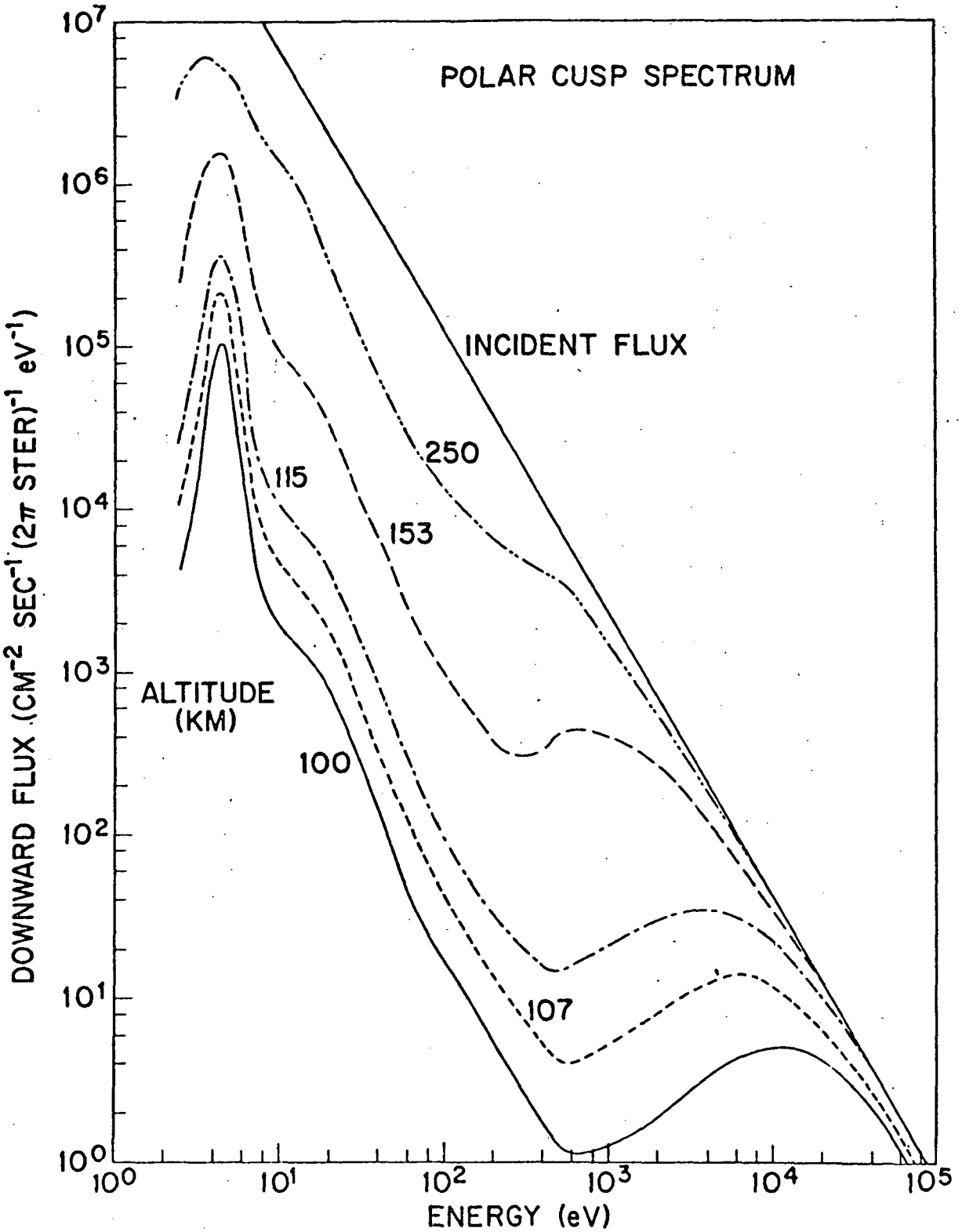
POLAR CUSP SPECTRUM
INCIDENT FLUX
250
153
115
100
107
ALTITUDE
(KM)
DOWNWARD FLUX (CM^{-2} SEC^{-1} (2π STER)$^{-1}$ eV^{-1})
ENERGY (eV)
10^0
10^1
10^2
10^3
10^4
10^5
10^6
10^7

Figure 16

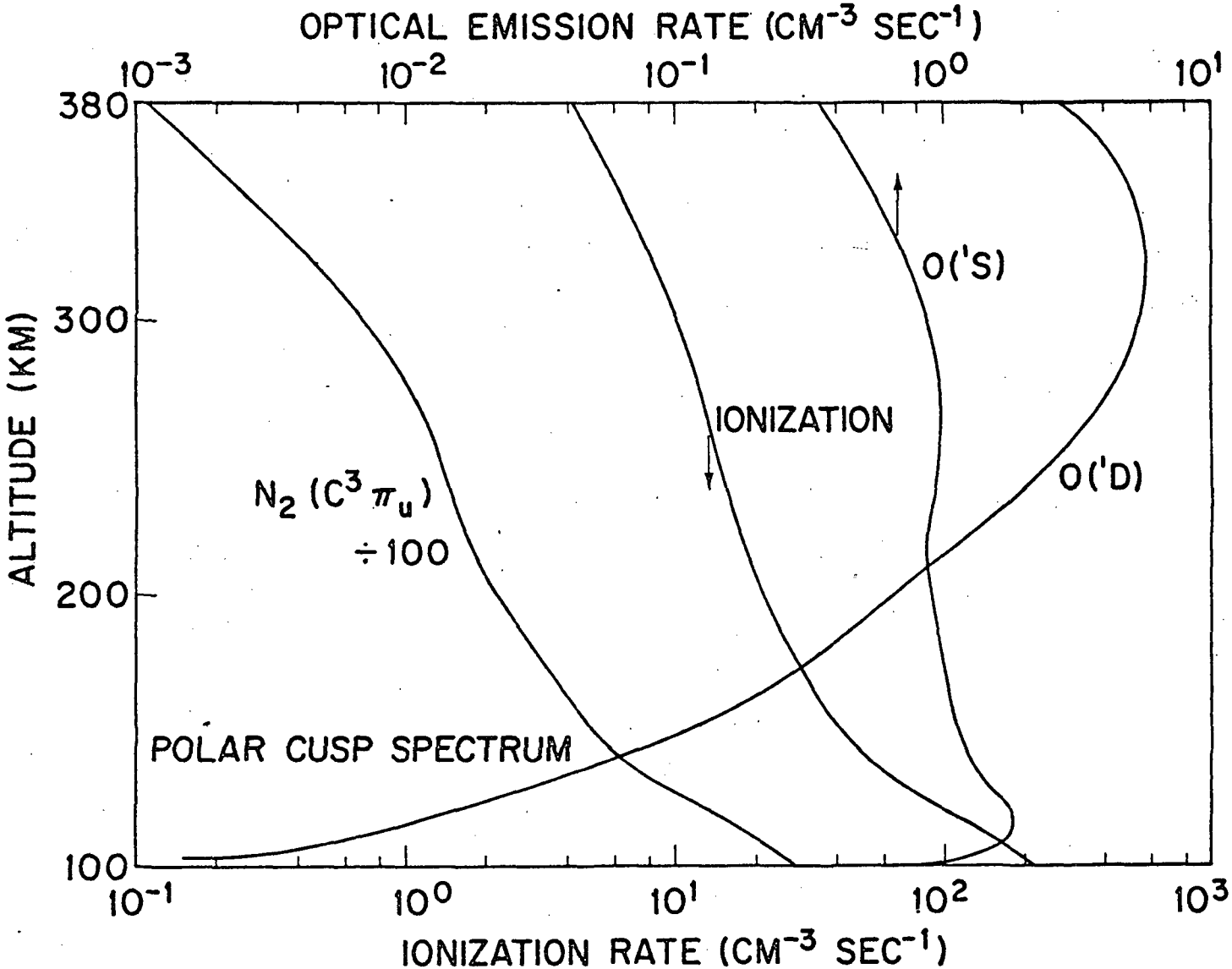
OPTICAL EMISSION RATE (CM^{-3} SEC^{-1})
10^{-3}
10^{-2}
10^{-1}
10^{0}
10^{1}
380
300
200
100
ALTITUDE (KM)
N_2 ($C^3\pi_u$)
÷100
IONIZATION
O('S)
O('D)
POLAR CUSP SPECTRUM
10^{-1}
10^{0}
10^{1}
10^{2}
10^{3}
IONIZATION RATE (CM^{-3} SEC^{-1})

Figure 17